1968-07

Interface shearing stress of a body in contact with water saturated sand

Gatlin, Carl Earl, Jr.

Cambridge, Massachusetts; Massachusetts Institute of Technology

INTERFACE SHEARING STRESS OF A BODY IN CONTACT WITH WATER SATURATED SAND

by

CARL EARL GATLIN, JR.

LIEUTENANT (JUNIOR GRADE), UNITED STATES NAVY

B.S., United States Naval Academy

(1967)

Submitted in Partial Fulfillment of the

Requirements for the Degree of

Master of Science in Naval Architecture

and Marine Engineering

at the

MASSACHUSETTS INSTITUTE OF TECHNOLOGY

July, 1968

Signature of Author: Carl Earl Gatlin, Jr.

Department of Naval Architecture and Marine Engineering, July 30, 1968

Certified by: S. Curtis Powell

Thesis Supervisor

Accepted by: _____

Chairman, Departmental Committee on Graduate Students

INTERFACE SHEARING STRESS OF A BODY IN CONTACT WITH WATER SATURATED SAND

by

CARL EARL GATLIN, JR.

LIEUTENANT (JUNIOR GRADE), UNITED STATES NAVY

Submitted to the Department of Naval Architecture and Marine Engineering on July 30, 1968, in partial fulfillment of the requirements for the Master of Science degree in Naval Architecture and Marine Engineering.

ABSTRACT

The reduction of shearing stress of a body in contact with sand was studied with the possible application of ungrounding ships. An annular ring with the thirty-six sources was rotated in a bed of sand so as to model an infinitely long ship with a series of pumps (sources) placed on the longitudinal centerline. By means of strain gages placed on four two-dimensional load cells, quantitative data for both normal and shearing stress were obtained. Also, by means of a pressure transducer, a type of strain gage, measurement of the pore water pressure was made. All three quantities: normal stress, shearing stress, and pore water pressure were thus measured simultaneously. Quantitative results showed that there was a reduction of 90% in shearing stress for a nominal value of pore water pressure (25-30 psi). These results were true for all three types of samples tested regardless of their initial coefficient of friction. The coefficient of friction was noted to decrease at higher pore water pressures giving rise to the idea that the dynamometer (force measuring device) may have deflected enough to negate the readings at higher pressures. Lending itself to this possibility was the fact that theoretical or predicted shearing stress was less than the measured stress at low values of pore pressure but greater than the measured stress at higher values of pore pressure. However, the overall results of the tests showed promising possibilities in reducing the number of salvage tugs, days to unground, etc., by employing a keel mounted pump. Suggestions are presented as to possible future research in this area.

Thesis Supervisor: S. Curtis Powell
Title: Associate Professor of Marine Engineering

ACKNOWLEDGEMENTS

The author wishes to thank:

Professor S. Curtis Powell for his guidance, help and understanding during the course of this work;

The U.S. Navy for its financial support;

Captain Robert E. Stark, USN (Ret.) and Commander Sherman C. Reed, USN, for their inspiration "to get the job done";

The technicians of the Materials Processing Laboratory whose help enabled the author to in fact, "get the job done."

Lieutenant Commander Samuel J. Gordon, USN, for his guidance and help throughout the entire year.

My wife, Linda, who put up with many more failures than successes.

TABLE OF CONTENTS

LIST OF FIGURES

LIST OF TABLES

LIST OF SYMBOLS

A	-	cross sectional area of flow, ft^2
b	-	width, in
c	-	cohesion
C	-	cohesive strength, no load shearing strength lb/in^2
E	-	modulus of elasticity
E_a	-	excitation voltage of transducer, V
E_o	-	output voltage of transducer, V
F	-	normal force, lb
k	-	stiffness, lb/in
K	-	coefficient of permeability, cm/sec
h	-	pressure head, ft
L	-	length of flow, ft
P	-	shearing force, lb
P_c	-	capacity pressure of transducer, lb/in^2
p_u	-	unknown pressure to be measured by transducer, lb/in^2
Q	-	flow rate, cm^3/sec
$Q(r)$	-	flow rate as a function of radial distance, cm^3/sec
$Q(s)$	-	flow rate as a function of lineal distance, cm^3/sec
r	-	radius, in
S	-	sensitivity of pressure transducer mV/V
S	-	shear strength, shearing resistance, or shearing stress, lb/in^2
t	-	thickness, in
$\tan \phi$	-	coefficient of friction
δ	-	deflection, in
ε	-	strain, in/in
γ	-	specific gravity of fresh water
μ	-	pore water pressure, lb/in^2
$\mu\varepsilon$	-	microstrain, 10^{-6} in/in
ϕ	-	angle of friction
σ	-	normal stress, lb/in^2
σ_t	-	total normal stress, lb/in^2
σ_e	-	effective or intergranular stress, lb/in^2
τ	-	shearing stress, lb/in^2

INTRODUCTION

In this report it will be found that three laws with various approximations governed the experimentation: Laplace's Equation, Coulomb's Law (Effective Stress Law), and Darcy's Law. However, before concerning oneself with exactly how these laws entered into the problem, it would be well to review some basic facts of civil engineering in general, and hydrology, in particular.

When speaking of shearing resistance, shearing stress, or shear strength (these terms were interchanged throughout this report), one should note that there are three conventional types of soil: (1) coarse grained or frictional, (2) fine grained or cohesive, (3) cohesive-frictional or ($c - \phi$). The maximum resistance to shearing stress is usually assumed to be of two parts: (1) internal friction or resistance due to interlocking of particles and (2) cohesion or the resistance due to forces tending to hold the particles together in a solid mass. Therefore, one can distinguish between coarse grained soils (e.g., sand) where they derive their total shearing strength from intergranular resistance and cohesive soils (e.g., clay) which tend to derive all of their shearing resistance from internal friction. The third category encompasses both of the above and tends to derive its total shearing strength from both internal friction and cohesion. It will be shown shortly the exact nature of the three shearing strengths so as to diminish any possibility of confusion which may now exist.

The coefficient of friction, a well known term found throughout the profession of engineering, assumes special importance in civil engineering. Consider a body with a normal force, W, and a shearing

force, S_f, acting on it. Then tan ϕ, the coefficient of friction, is equal to S_f divided by W.

$$\tan \phi = \frac{S_f}{W} \qquad (1)$$

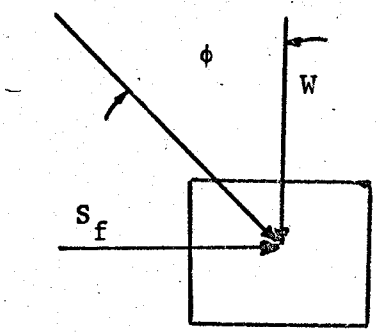

FIGURE I.

DIAGRAM OF THE COEFFICIENT OF FRICTION

ϕ is sometimes referred to as the friction angle and is the angle with the horizontal which a mound of soil makes when poured freely. Furthermore, the friction angle is a function of the type of soil and such factors as moisture content, density and degree of consolidation.

It would now be appropriate to express Coulomb's Law which was stated by C. A. Coulomb in 1776, and was the first formal hypothesis dealing with the frictional resistance of earth masses. Coulomb's Law states that the shear strength of purely frictional soil is proportional to the normal forces on the plane of shear. Therefore, the law governing shear failure of solids states that:

$$S = C + \sigma \cdot \tan \phi \qquad (2)$$

where S = shear strength of shearing stress

C = apparent cohesion

ϕ = angle of friction

σ = normal stress

A diagram of Coulomb's empirical equation would look like this:

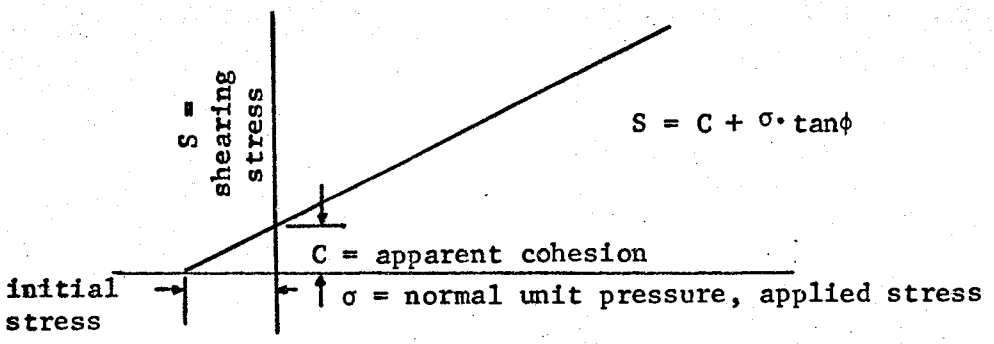

FIGURE II

Thus, one can see that cohesive soil has a finite shearing strength (equal to C), even when not subjected to external forces normal to the shear plane. That portion of shearing strength which is independent of normal pressure is called "cohesion" or the "no load shearing strength." A good example of cohesion is two sheets of fly paper with the sticky sides in contact. The cohesion component is usually furnished by the fine fractions of the soil such as silt, clay, and inorganic colloidal material. Cohesion may also be furnished by moisture films and bituminous binders (e.g., asphalt and tar). One may wonder why the name "apparent" is attached to the word cohesion. In the case of soil, the capillary

pores set up compressive stresses in the soil skeleton which are directed inward and which contribute to the strength and stability of the soil mass. Capillary - induced strength is temporary and may disappear when the soil is saturated. It happens that highly capillary solids exhibit considerable cohesive shearing strength when partially saturated with water, because of compressive forces supplied by capillary menisci and is called "apparent" cohesion. This is lost when the soil is saturated, since saturation eliminates capillary menisci and associated capillary forces. Thus, the residual cohesion in a saturated soil is "true" cohesion.

Before leaving the subject of cohesion for good, a comparison (in the form of diagrams) of the three categories of soil will be drawn to elucidate Coulomb's Law:

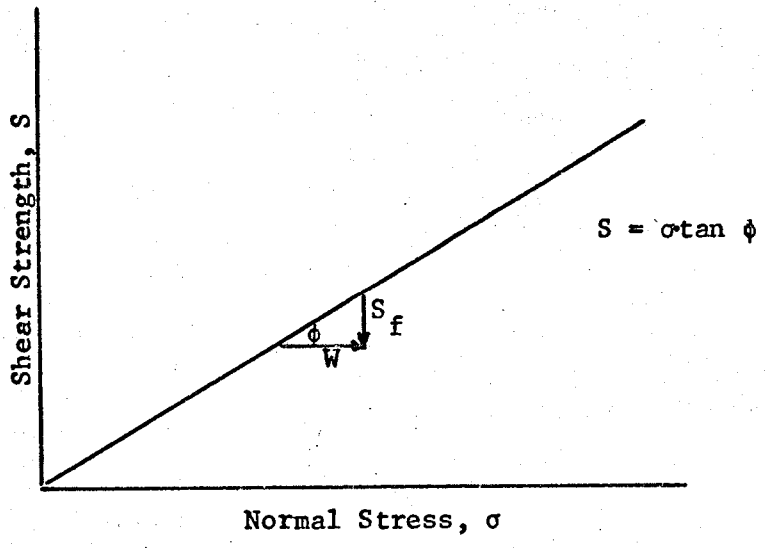

FIGURE III

COARSE GRAINED OR FRICTIONAL SOIL (1)

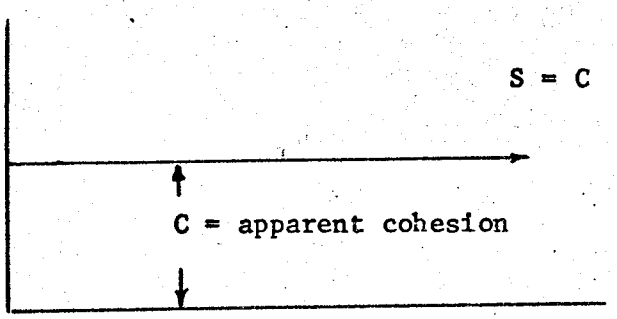

FIGURE IV

FINE GRAINED OR COHESIVE SOIL (1)

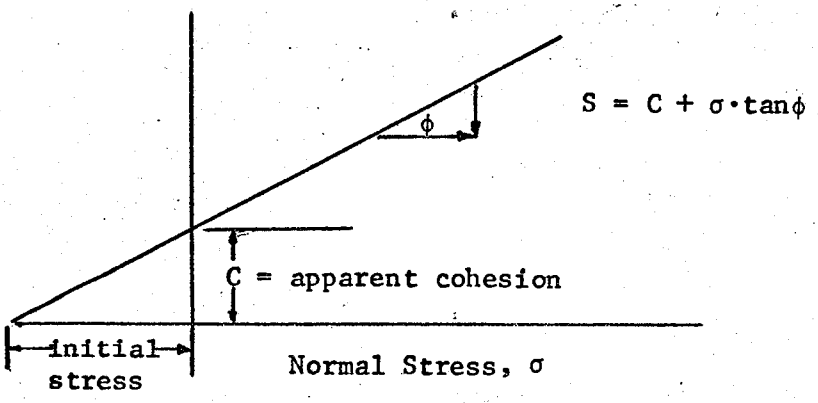

FIGURE V. COHESIVE-FRICTIONAL OR (C-ϕ) SOIL (1)

Turning once again to Coulomb's Law, there will be derived from it what is often referred to in the profession as the "Effective Stress Law." It is sometimes incorrectly assumed that the total normal stress, σ_t, acting on the shear plane governs the strength of the soil. But the application of normal stress results in a temporary increase in the pore-water pressure, and effective or intergranular stress is given by σ_e,

on which shear strength depends or

$$\sigma_e = \sigma_t - \mu \quad . \tag{3}$$

where μ = pore water pressure.

That is to say that part of the load which was formerly borne by the soil is, upon the addition of water, subsequently borne by the water. Therefore, a more fundamental form of Coulomb's Law may be given as

$$S = C + (\sigma_t - \mu)\tan \phi \tag{4}$$

or for cohesionless sand,

$$S = (\sigma_t - \mu)\tan \phi \tag{5}$$

$$S = \sigma_e \tan \phi \tag{6}$$

In the experimentation, the pore water pressure was measured by a pressure transducer located over the ring of sources, and it can be easily seen that the pressure head at this point is

$$h = \frac{\sigma_t - \sigma_e}{\gamma} = \frac{\mu}{\gamma} \tag{7}$$

where h = head

μ = pore water pressure

σ_t = total applied stress

γ = specific gravity of fresh water

γ = 62.4 lbf./ft.^{3}

Following the development of the other two laws the Effective Stress Law was reconsidered in the part it played in the development of predicting the shearing resistance of a body in contact with sand.

Next was considered the equation of Laplace and the fact that the flow of ground water through a soil obeys the same law as does phenomena in other branches of mathematical physics - in the steady conduction of electricity and heat, in steady diffusion, and in the theory of elastic membranes.

Thus, in those cases of steady flow where the velocity distribution, and hence the pressure distribution, does not change with time, the approximate partial differential equation for the steady flow of water in a homogeneous and isotropic material is therefore

$$\frac{\partial^2 h}{\partial x^2} + \frac{\partial^2 h}{\partial y^2} + \frac{\partial^2 h}{\partial z^2} = 0 \quad . \tag{8}$$

The assumption is made, of course, that the fluid is irrotational and incompressible.

Now the flow can be reduced to a two-dimensional problem of flow in a horizontal plane if it is assumed the water is flowing steadily in a sand of uniform thickness. While this was not the exact case at hand during

the experimentation, it was felt that the assumption can be made with little error since the flow elsewhere was negligible compared to that through the uniform stratum. If the lateral boundaries of the sand are vertical and if conditions on those boundaries are vertically uniform, the flow takes place in parallel planes. As is usually the case, if the slope of the sand is small, then it may be assumed that the vertical component is everywhere zero. Hence, Eqn. (8) reduces to the two-dimensional Laplace equation,

$$\frac{\partial^2 h}{\partial x^2} + \frac{\partial^2 h}{\partial y^2} = 0 \quad . \tag{9}$$

In 1856, Henry Darcy, a French hydraulic engineer discovered the law which governs the flow of water or of other viscous liquids through porous materials which they saturate. By investigating the flow of water downward through horizontal filter beds discharging at atmospheric pressure he verified what is now called Darcy's Law. Thus, for sufficiently low rates of flow the discharge, Q, varies directly with the loss of head $h_1 - h_2$, or

$$Q = \frac{KA(h_1 - h_2)}{L} \tag{10}$$

where h_1 = inflow head

h_2 = outflow head

L = length of flow

A = cross-sectional area

K = permeability constant

Diagramatically, Darcy's Law would follow a case such as that illustrated below:

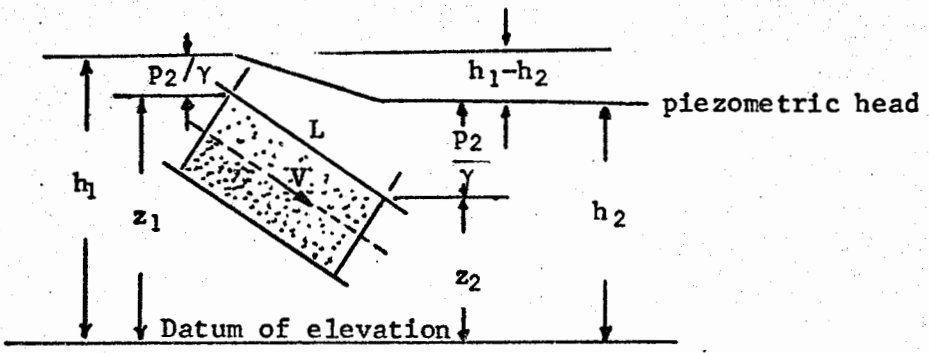

FIGURE VI

HEAD AND PRESSURE DISTRIBUTION IN
UNIFORM LAMINAR FLOW THROUGH SAND (12)

Proceeding now to generalize Darcy's Law for the situation involved in this report, consider the unidirectional case where the head loss may be assumed to be uniformly distributed along the direction of flow. On a macroscopic scale, that is, if the mean head is taken at different points along a given streamline, the gradient of this average head will be more or less uniform. Summing several of these flows along several of these streamlines, it will be found that they are also uniform. For this reason, a mathematical continuum may be substituted for the physical system. Therefore Darcy's Law may be written as

$$Q(s) = KA\frac{\partial h}{\partial s} \qquad (11)$$

where Q(s) and h are continuous functions of s, the distance along the average direction of flow.

Equation (11) may be transformed into polar coordinates as follows:

$$Q(r) = 2\pi r K h \frac{\partial h}{\partial r} \tag{12}$$

Integrating and evaluating the resultant constant by noting that at $r = r_{sink}$, it follows that $h = h_{sink}$, then

$$Q \ln r \Big|_{r_{sink}}^{r_{source}} = 2\pi K \frac{h^2}{2} \Big|_{h_{sink}}^{h_{source}} + C \tag{13}$$

and evaluating the constant of integration

$$Q \ln \frac{r_{source}}{r_{sink}} = \frac{2\pi K}{2} \left| h^2_{source} - h^2_{sink} \right| \tag{14}$$

In the case of experimentation for this report the head, h, was assumed to be known at two points: (1) at the sink, since the water was discharged at atmospheric pressure, and (2) the location of the sources, since the pore water pressure was measured there with the transducer. It was assumed that there was negligible head loss between the one-quarter inch of sand sample separating the point of the source and the pressure transducer. Also, the assumption was made that there was negligible head loss between the point of the sink and the point of atmospheric discharge, although this was most certainly incorrect.

For a given sample of sand, two aspects were immediately known. First, the coefficient of friction tan ϕ, was either known or easily

measured for a saturated sample when there was no flow. Secondly, the coefficient of permeability was measured, albeit very roughly, and likewise has been tabulated (12, p.48) for various types of grain sizes for soils (e.g., gravel, gravel mixed with sand, coarse sand, etc.). Therefore, in this report a rough calculation (see Results) of the coefficient of permeability was made and compared to that which was tabulated, and also in some cases to that which was calculated by LCDR. S. J. Gordon, USN.

Referring to Figs. VIII and IX in the Procedure, the radial measurements of the source and sink were known. Consequently, the only remaining factor to be determined was the flow rate which was easily measured with a stop watch and a beaker of known volume.

Thus, in summation, the following items are known:

Q = flow rate, measured

r_{source} = 3 inches, measured

r_{sink} = 11/16 inches, measured

h_{source} = head at source, measured with pressure tranducer

h_{sink} = head at sink = 0 since discharging to atmos.

Solving Eqn. (14) for K, the coefficient of permeability

$$K = \frac{Q \ln r_{source}}{\pi \quad r_{sink}} \times \frac{1}{h^2_{source}} \qquad (15)$$

$$\ln \frac{r_{source}}{r_{sink}} = \frac{\ln 3}{11/16} = \frac{\ln 48}{11} = 1.47$$

or

$$K = 0.468\ Q \times \frac{1}{h^2_{source}}$$

Keep in mind, however, that K will be used only to get a rough idea of just how reasonable are the other factors involved. Coulomb's Effective Stress Law still holds and will be used exclusively to predict the shearing stress. As will be shown in the Results, there were enough unknowns and sources of error to negate the possibility of really using any calculated value of K.

Going back to Eqn. (14) and solving for the head at the source

$$\pi K h^2_{source} = Q \ln \frac{r_{source}}{r_{sink}} + \pi K h^2_{sink}^{0} \tag{16}$$

or

$$h^2_{source} = \frac{Q \ln r_{source}}{\pi K \quad r_{sink}} \tag{17}$$

hence

$$h_{source} = \frac{Q}{\pi K} \ln \frac{r_{source}}{r_{sink}} \tag{18}$$

Two things should be brought to mind at this point. One, there is a unique distribution of head for a given radius since only the positive value of the square root was used. Next, a unique head distribution is determined for any given flow rate, and thus for an infinite number of flow rates there would have been an infinite number of head distributions.

Returning now to the Effective Stress Law and recalling that

$$\sigma_e = \sigma_t - \mu \tag{3}$$

where once again σ_e = effective stress

σ_t = total, applied stress

μ = pore water pressure

and finally,

$$S = \sigma_e \tan \phi \tag{6}$$

Thus, by knowing the normal stress and the pore water pressure, which were both measured values in this case, the shearing stress was then capable of being determined. But, the shearing stress was also a function of the head distribution, since,

$$\sigma_e = \sigma_t - \mu \tag{3}$$

and

$$h = \frac{\mu}{\gamma} \tag{7}$$

Thus, given a flow rate, there is a unique head, and hence, shear stress distribution along a radial line extending from the center of the sink outward to the sources.

In the experimentation the four load cells of the torsion dynamometer measured the torque over a circular annulus with an inner diameter of five and three-fourths inches and an outer diameter of six and one-fourth inches. But since the torque over this annulus was nothing more than the shearing force times the mean radius, one was able to immediately determine the shearing stress (the force divided by the area of the annulus). Thus for a particular flow rate it has already been stated that we indirectly know the theoretical or predicted shear stress, and the actual or measured stress can now be compared.

That there was a discrepancy between the two evolves from the fact that the theoretical stress was predicted for a radius of three

inches (the mean radius), and the natural logarithm is not a straight line plot between the outer and inner radius. That is to say if the logarithm of one-half the outer radius (of the annulus) divided by the sink radius plus the logarithm of one-half the inner radius divided by the sink radius were equal to the logarithm of the mean radius of the annulus divided by the sink radius, and no other errors were introduced, then one should have expected the measured and predicted shearing stresses to be identical values. The above is probably more easily seen mathematically.

$$\ln\left[\frac{\left(\frac{2\ 7/8}{11/8}\right)}{2}\right] + \ln\left[\frac{\left(\frac{3\ 1/8}{11/8}\right)}{2}\right] = \ln\left[\frac{\left(\frac{23/8}{11/8}\right)}{2}\right] + \ln\left[\frac{\left(\frac{25/8}{11/8}\right)}{2}\right]$$

$$= \ln\left[\frac{23/8 \times 25/8}{(11/8)^2}\right]^{1/2}$$

$$= \ln\left[\frac{(23 \times 25)/64}{(11/8)^2}\right]^{1/2}$$

$$= \ln\left[\frac{(575)/64}{(11/8)^2}\right]^{1/2}$$

$$= \ln\left[\frac{3}{(11/8)}\right] = \ln\left[\frac{24/8}{11/8}\right]$$

As $\left[\frac{24}{8}\right]^2 = \frac{576}{64} \neq \frac{575}{64}$, it is easily seen that an error of 1/64 was introduced. However, compared to some of the other errors necessarily incurred during the course of this report, 1/64 was negligible.

PROCEDURE

A very general description of the testing apparatus will be given in the first part of this section with more detailed specifications and descriptions given in the Appendix. The testing apparatus was simple in concept, although it was plagued by limitations on one of the measuring devices and an almost fixed flow rate. These will be discussed in greater detail later in the paper.

Basically, a sample of sand of non-uniform thickness was placed in a confined chamber consisting of a circular outer sleeve or collar, the top plate or torsion dynamometer, and the bottom plate containing the ring of sources which gave the sample the non-uniform thickness, (see Figs. VII and VIII). The three aforementioned articles when assembled were mounted on a milling machine with rotary table commonly found in a machine shop. However, in place of the hand crank an electric motor with a variable speed drive was installed.

The top plate assembly consisted of three circular annuli. Located symetrically in the inner annulus was the sink consisting of nothing more than a center tap with a sintered bronze filter to prevent the sand from escaping the chamber. Dimensions of the inner annulus can be found from Fig. IX.

The middle annulus assembly contained the heart of the measuring devices which will be discussed in detail. Used for measuring normal stress and shearing stress were four octagonally shaped load cells upon which were mounted sixteen strain gages. A complete discussion of the strain gages, load cells, and the annulus itself with dimensions, construction, specifications, etc. will be found in the Appendix and Fig. IX. Also located on the middle annulus assembly was the pore water pressure transducer pictured in Fig. X.

FIGURE VII

TOP AND BOTTOM PLATE ASSEMBLY

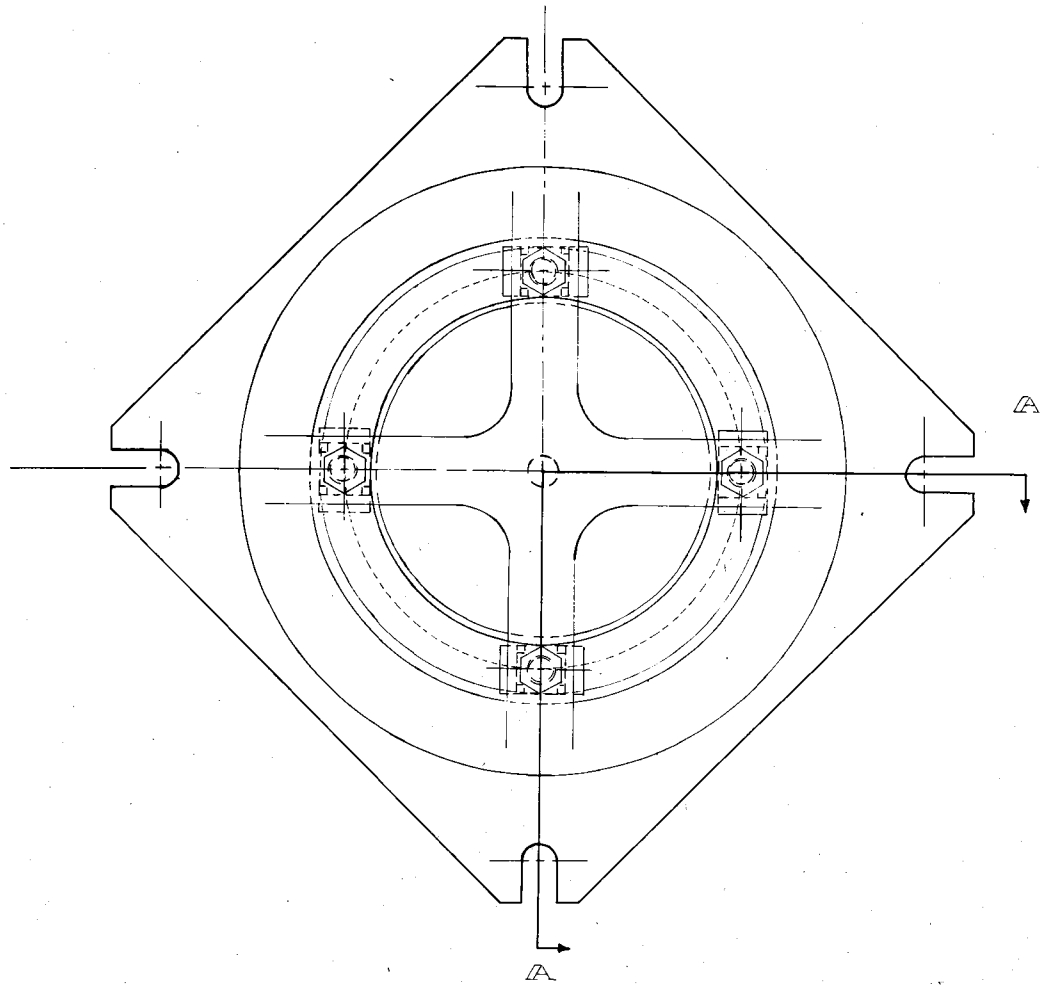

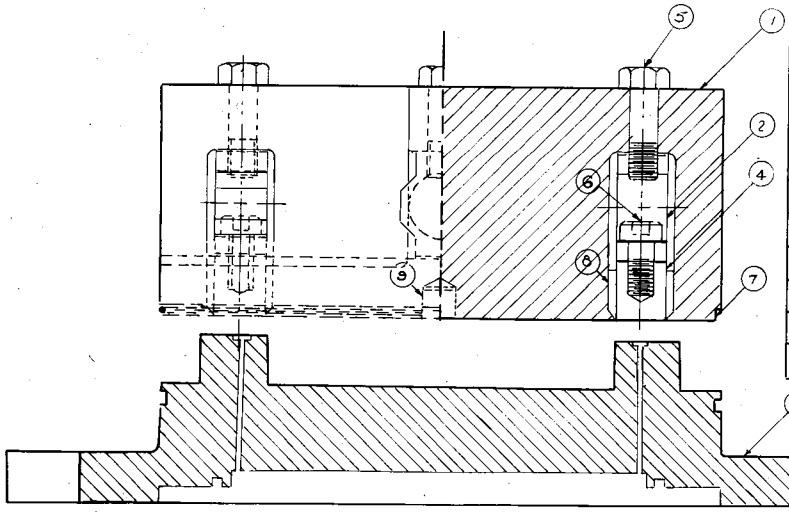

NO.	DESCRIPTION	REQD	MAT'L
1	BODY	1	ALUM.
2	LOAD RINGS	4	STL.
3	BASE	1	ALUM.
4	RING	1	ALUM.
5	7/16 - 20 HEX HEAD	4	STD. STK.
6	5/8 - 24 ALLEN HEAD	4	STD. STK.
7	'O' RING SEAL	1	STD. STK.
8	TUBE - RUBBER SEALANT	1	STD. STK.
9	DRAIN	1	STL

SECTION A-A

FIGURE VIII

BOTTOM PLATE ASSEMBLY

WITH DIMENSIONS IN INCHES

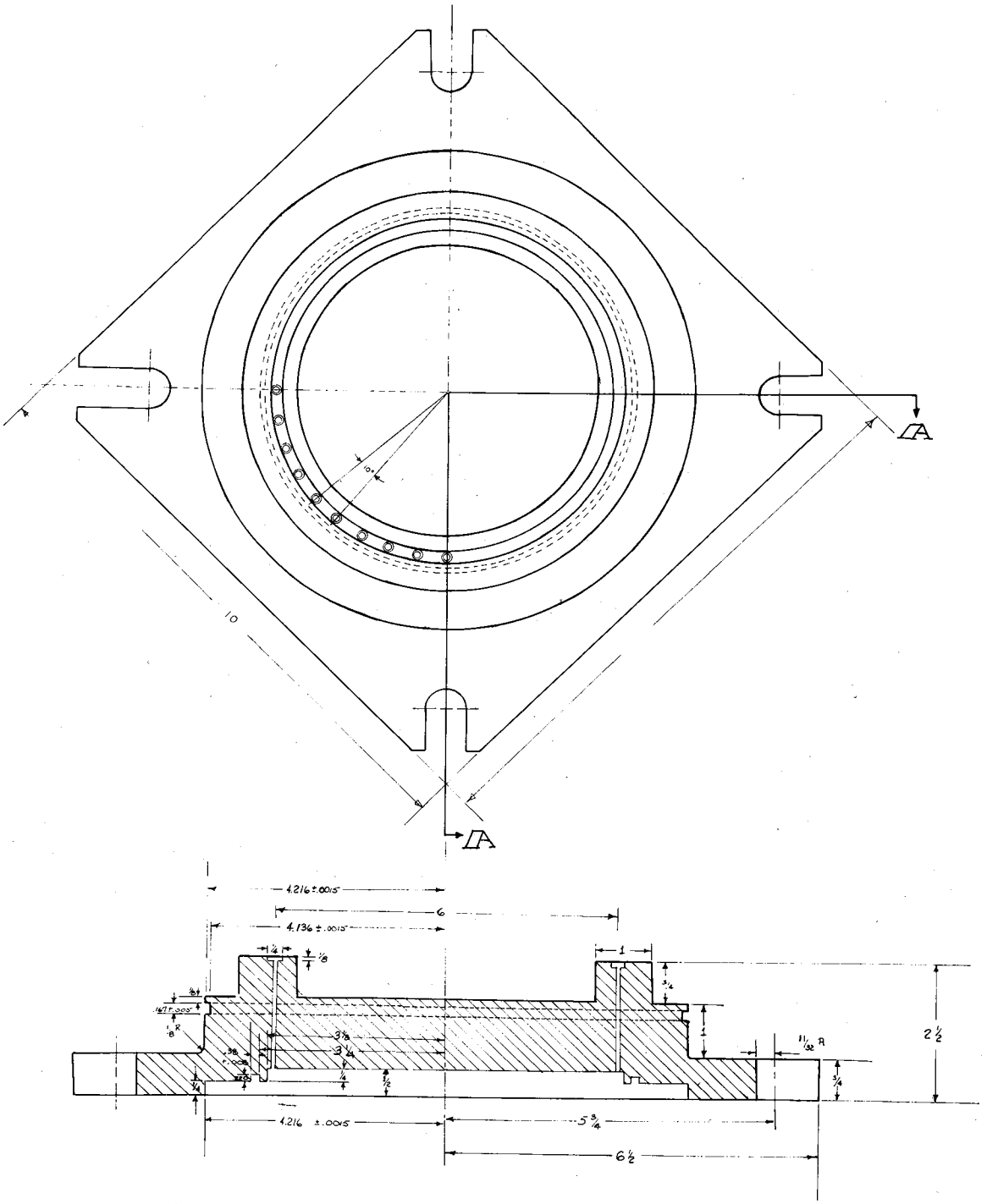
A
A
10°
10
4.216 ± .0015
6
4.136 ± .0015
1/4
1/8
1
3/4
1
1/8 R
3 3/8
3 1/4
11/32 R
2 1/2
1/4
1/2
3/4
4.216 ± .0015
5 3/4
6 1/2

FIGURE IX

TOP PLATE ASSEMBLY

WITH DIMENSIONS IN INCHES

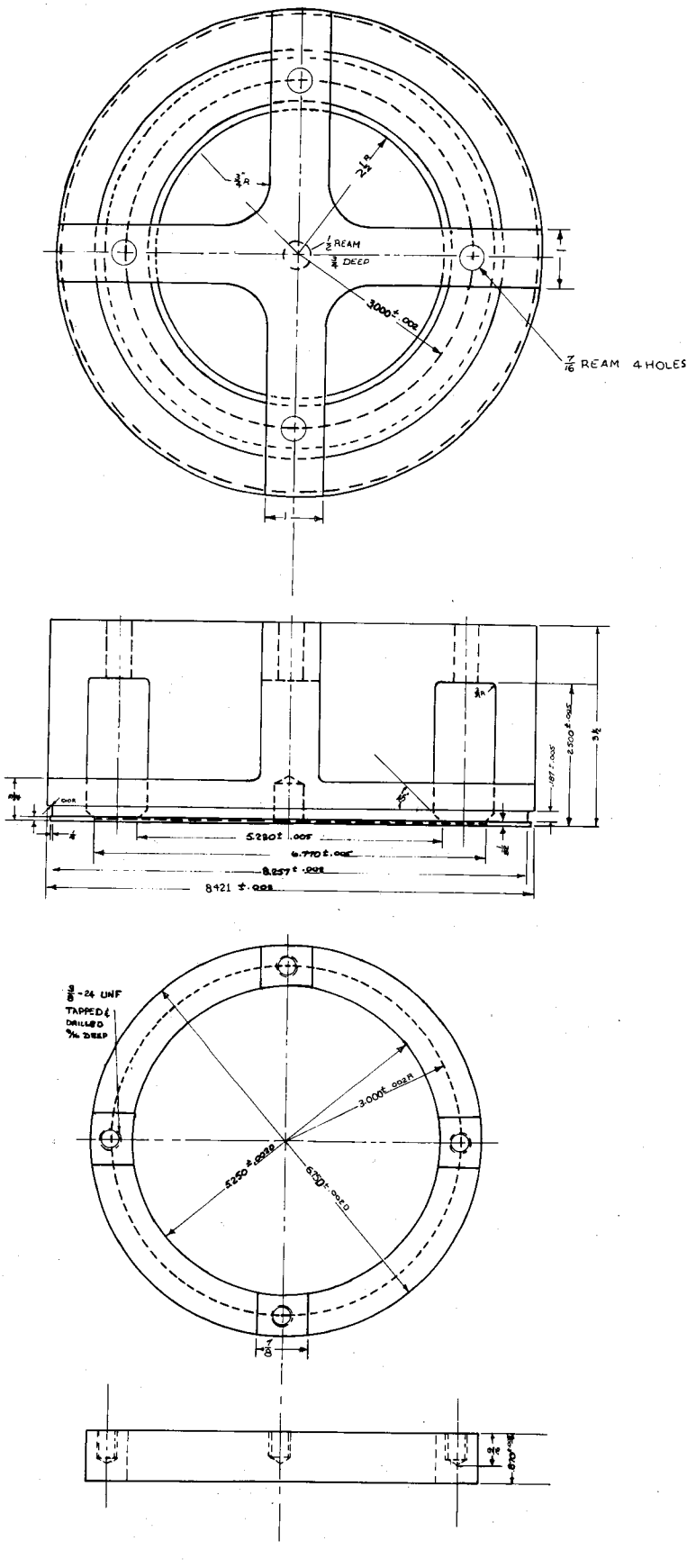
3000± .005
7/16 REAM 4 HOLES
5.280± .005
6.710± .005
8.257± .005
8421 ± .005
3/8-24 UNF
TAPPED &
DRILLED
9/16 DEEP
3.000± .005R
4.250 ± .0020
6.000± .005D

Fig. 10a. Test apparatus mounted on milling machine.

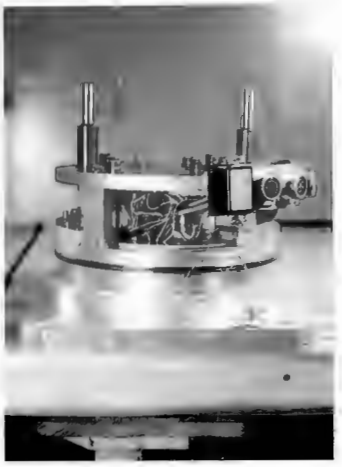

Fig. 10b. Top and bottom plate assembly with pore water pressure transducer lying to the right.

Fig. 10c. Close-up of test apparatus.

Fig. 10d. Left to right: collar, bottom plate assembly showing source ring, and top plate assembly showing annular rings with pore water pressure transducer in front.

FIGURE X

The last part of the top plate assembly not yet considered is the outer annulus. Its only actual importance was to give the top plate assembly the desired diameter and further, was the location of the double '0' ring between the top plate and the cylinder.

The cylindrical sleeve or collar was of steel construction and was bored out to a tolerance of 0.003 inches. (See also Fig. X).

The bottom plate consisted of a raised annular ring of sources which led to the non-uniformity in the thickness of the sample. The annulus contained thirty-six equally spaced sources of one-eighth inch diameter and were tapped from a common collecting chamber for the incoming water. (See Fig. VIII). The concentrically mounted bottom plate was mounted on the rotary table so as to prevent any eccentricity in rotation. The final positioning was done by using a dial indicator which was stationary as both the rotary table and the bottom plate were rotated. A tolerance of about 0.001 inches was allowed as this was less than the 0.003 tolerance between the sleeve and the top plate. Note that the sleeve was mounted on the bottom plate with three set screws approximately 120° apart, and thus became a rotating member during testing. Tapped into the water chamber of the bottom plate was a three-eighth inch pipe diameter swivel joint which permitted rotation of the bottom plate assembly with respect to the copper tubing soldered below the joint. Thus, unwinding of flexible hose or the shearing off the connecting pipe was prevented. As the outside diameter of the swivel joint was 1/8" less than the hole diameter of the rotary table, the swivel joint was able to extend below the top surface of the table. The hole of the rotary table was continuous, thus allowing copper tubing to be led down from the rotary table. By the use of fittings, a globe valve was installed to permit easier and "on location"

control of the flow rate and water pressure.

Cold tap water with a pressure between 45 and 50 psig was used. However, the capacity of the pore water pressure transducer was only 25 psig (see Appendix). Therefore, the pressure of the water had to be carefully monitored so as to prevent damage to the transducer. Even with the great number of valves, elbows, constrictions in flow, etc., the velocity of flow was so low that the head losses were negligible. Also it was noted a large amount of air was present in the water causing fluctuations in some pore pressure readings, and was a possible cause of slight pitting of the bottom surface of the top plate.

Ottawa 20-30 sand was used throughout the testing, except in the case where the glass beads were used. The sand was first filtered through a series of three U.S. Standard Sieve Series strainers (see Appendix - Table X for specifications) giving four approximately equal filtered grain sizes that could be used. However, only the two coarsest (largest) filtered grain sizes were used.

The test chamber held roughly 1000 gms of water saturated sand. After the top surface of the sand and water mixture was carefully smoothed out, the rotary table was raised into position, with the sample just out of contact with the torsion dynamometer (bottom surface of the top plate assembly).

At this point, the recorders and oscilloscopes were balanced, primarily so that there would be a common zero for all attenuator settings. Also, the excitation voltage was checked for the pore water pressure transducer, as this varied the output somewhat (see Eqn. (26), Appendix).

The rotary table with the mounted bottom plate was then raised until some of the excess water was forced out through the opening for

the pore water pressure transducer. After inserting and securing the pressure transducer the test was ready to begin. The readings of normal and shearing stress, plus pore water pressure were checked to make sure they were initially zero.

After having started rotation, the table was raised at 0.005 inch increments until it became obvious that any further increase in table position would overload the electric motor and stop rotation. Note that throughout this first portion of the testing, there was no flow of water into the sample. However, upon final positioning of the sample when it had become obvious that the sand sample was in contact with the dynamometer, water flow was begun. Great care had to be taken to insure that the pressure of this inflowing water did not exceed the capacity of the pore water pressure transducer, as this was one of the serious limitations mentioned earlier in this section.

There was almost no control over the rate of flow as the impedance of the sand to the flow of water was extremely great (see Results), and normally only a trickle was observed. Another limitation in the experimentation was the necessarily small tubing used to transport the water to the sample. The tolerances of the milling machine under the rotary table were such that only 3/8" diameter or less copper tubing had to be used. However, as mentioned later in the paper, the flow rate was not as important as the higher pressure.

The complete range of pressures between 0 and 25 psi were tested to get some idea of the variation of shearing stress with pore water pressure. Also, the range of speeds of ratation (0 to 40 rpm) was tested, and without trying to jump ahead, it was found that rate of shear had no effect on the magnitude of the shearing stress.

RESULTS

Unfortunately, no simple well defined number or equation will evolve from the next three sections, but rather a somewhat generalized explanation will be forwarded. As stated previously, three types of samples were tested: glass beads, and two homogeneous samples of Ottawa 20-30 sand, both rather coarse grained.

As was promised in the Introduction, a sample calculation will be given comparing the coefficient of permeability that was calculated to that which was "categorized" by Terzaghi and Peck [12, p.48]. That is, for highly permeable soil K varies between 100 and 10^{-4} cm/sec, while for soils of poor permeability, K varies between 10^{-4} and 10^{-6} cm/sec, and for anything below 10^{-6} cm/sec the soil is considered practically impervious. Gordon also calculated the permeability for glass beads in his thesis, and it was about 50 times that calculated in this paper. This is not surprising, however, as he applied a known back pressure at the sink, whereas in this paper the head at the sink was erroneously assumed to be zero (the exact head at the sink was pure conjecture).

From Eqn. (14)

$$Q \ln \frac{r_{source}}{r_{sink}} = \pi K h^2_{source}$$

measured values: $r_1 = 11/16"$

$r_2 = 3"$

$Q = 8$ ml/sec $= 8$ cm^3/sec

$$h_{source} = \frac{25 \text{ psig}}{62.4 \text{ lb/ft}^3} = 57.75 \text{ ft.}$$

therefore

$$K = \frac{8\ cm^3}{sec} \times \frac{1.47}{3.14} \times \left(\frac{1}{57.75\ ft}\right)^2 \times \frac{1}{144\ in^2/ft^2} \times \left(\frac{1}{2.54\ cm/in}\right)^2$$

$$K = 1.38 \times 10^{-5}\ cm/sec$$

Gordon calculated K to be 6.7×10^{-4} cm/sec, which is just barely in the category of soils that have good permeability. Further, Gordon had virutally no air in his sample, whereas in this case, a great deal of air was introduced reducing the calculated permeability of the soil [12,p.46].

In a similar manner, the permeabilities of the two samples of sand were found to be:

$K = 4.94 \times 10^{-6}$ cm/sec coarser grained

$K = 5.74 \times 10^{-7}$ cm/sec finer grained

and the computation was subject to the same sources of error that was evident in the case of the glass beads.

With the hope of getting some idea of just what the response of shearing stress to normal load, a test was made in which the table was raised in increments of 0.005 inches (See Figs. XI-XIII). The tests were conducted on water saturated samples, but the pore water pressure was maintained at zero. Thus, the non-rigidity of the system was somewhat mitigated. The results showed that once the top plate assembly was fully in contact with the soil, the ratio of shearing stress to normal stress (coefficient of friction) remained constant for a zero-flow rate condition. Likewise, the results of the test pointed to the necessity of

maintaining contact with the soil for any worthwhile data. Once it was evident that any further increase in table position would cause rotation to cease the other tests to be conducted on the sample were then begun with the knowledge that all of the excess water had been forced out. In forcing out this excess water, each test was started from almost the same point of reference; that is, each sample was saturated, but not to an excess, with water.

Once the testing of shearing stress vs. table position had been completed on each individual sample, the primary test in the experimentation of this report was then conducted which was the response of shearing stress with changes in the pore water pressure of a body in contact with sand. Although no curve fitting empirical equation can be advanced, it is seen from Fig. XIV - XVI that without exception, an increase in the pore water pressure caused a corresponding reduction in the shearing stress. This observation will be reviewed in the next section.

Probably, the most noticeable fact at a first glance was the fact that the coefficient of friction did not remain constant. That is, the value of τ_{meas}/τ_{pred} should have been 1.0. However, the ratio ranged in value from 1.0 to 0.3 for the finer grained sample. The glass beads contained quite a few points that were "believed" to be in error and were therefore not considered. For the others τ_{meas}/τ_{pred} again ranged from 1.0 to 0.3.

As the "apparent" coefficient of friction did not remain fixed, the total normal and effective stress varied somewhat. For example, the effective stress should have gone to zero as soon as the pore water pressure was increased to a point beyond the total normal stress. However, the value of σ_t also increased as the pore water pressure was

raised, although at a slower rate.

Finally, note that for the coarser-grained sand sample, the 25 psi limit on the pore water pressure was inadvertently exceeded. However, the results showed that above 30 psi, there was no great reduction in shearing stress, suggesting that there could be a limit of favorable reduction of shearing stress.

FIGURE XI

SHEARING STRESS VS. TABLE POSITION

IN 0.005 INCH INCREMENTS

FOR FINER GRAINED SAND

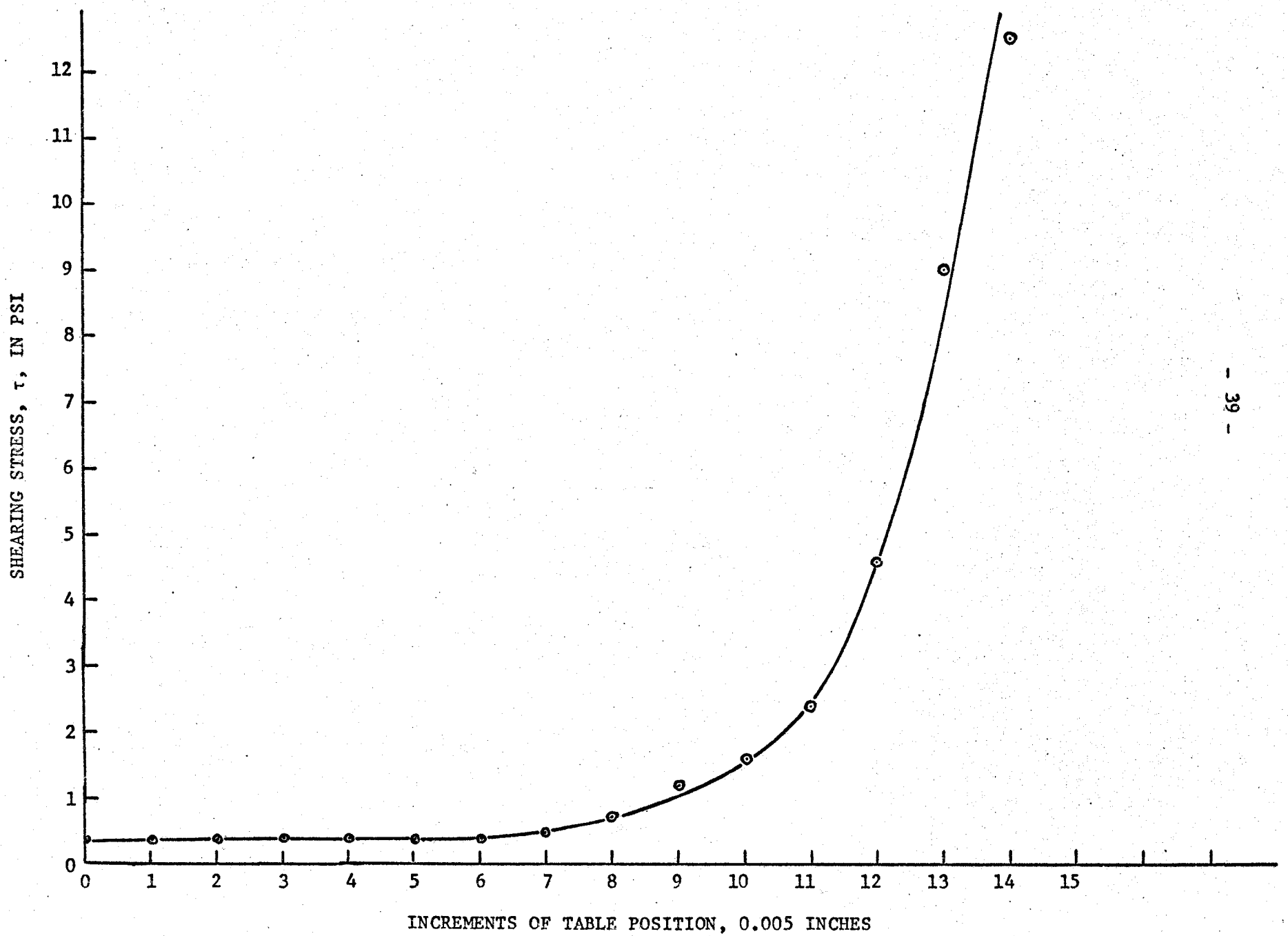
SHEARING STRESS, τ, IN PSI
0
1
2
3
4
5
6
7
8
9
10
11
12
0
1
2
3
4
5
6
7
8
9
10
11
12
13
14
15
INCREMENTS OF TABLE POSITION, 0.005 INCHES

FIGURE XII

SHEARING STRESS VS. TABLE POSITION

FOR COARSE GRAINED SAND

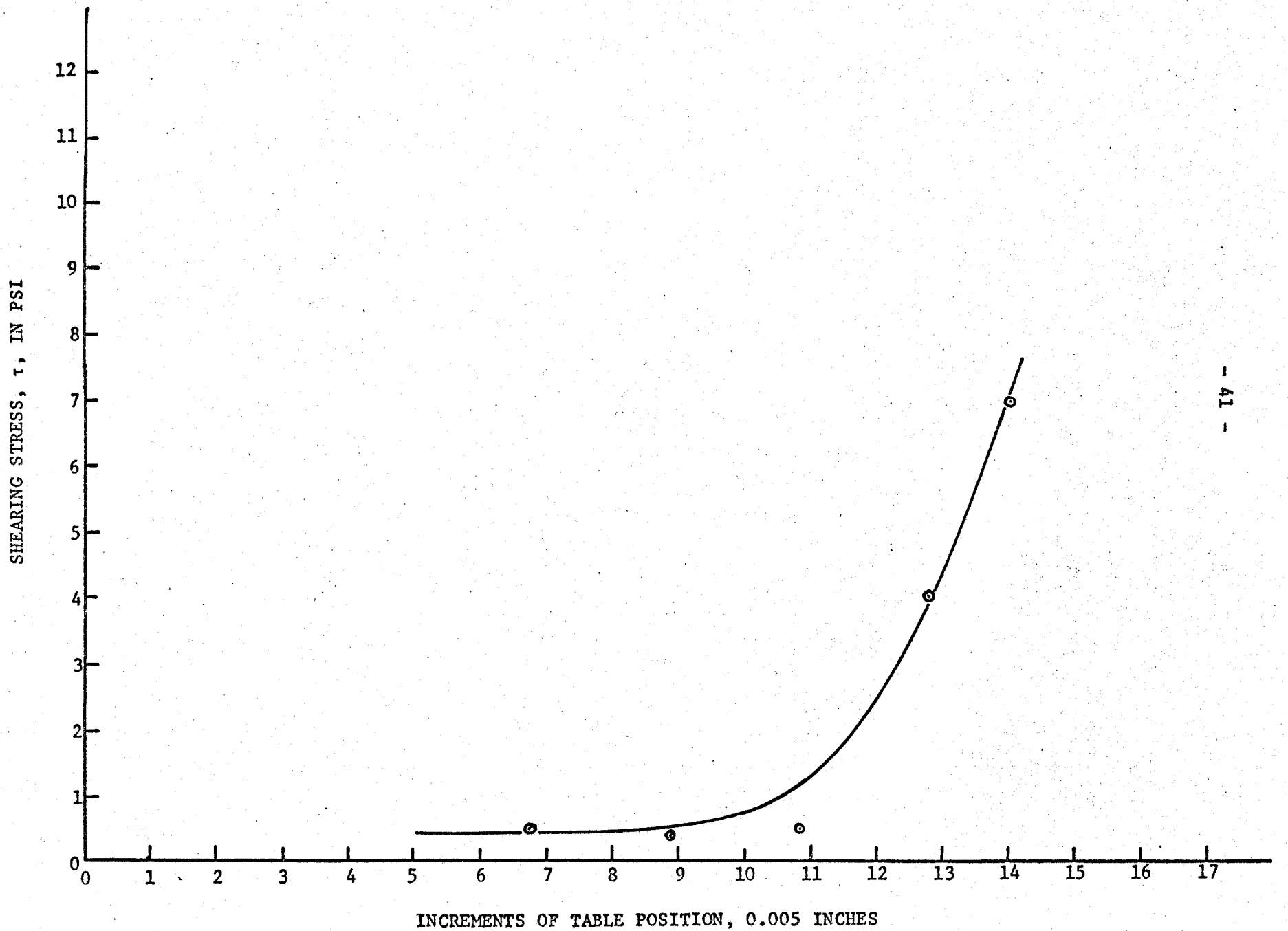
SHEARING STRESS, τ, IN PSI
0
1
2
3
4
5
6
7
8
9
10
11
12
0
1
2
3
4
5
6
7
8
9
10
11
12
13
14
15
16
17
INCREMENTS OF TABLE POSITION, 0.005 INCHES

FIGURE XIII

SHEARING STRESS VS. TABLE POSITION

AT INCREMENTS OF 0.005 INCHES

FOR GLASS BEADS

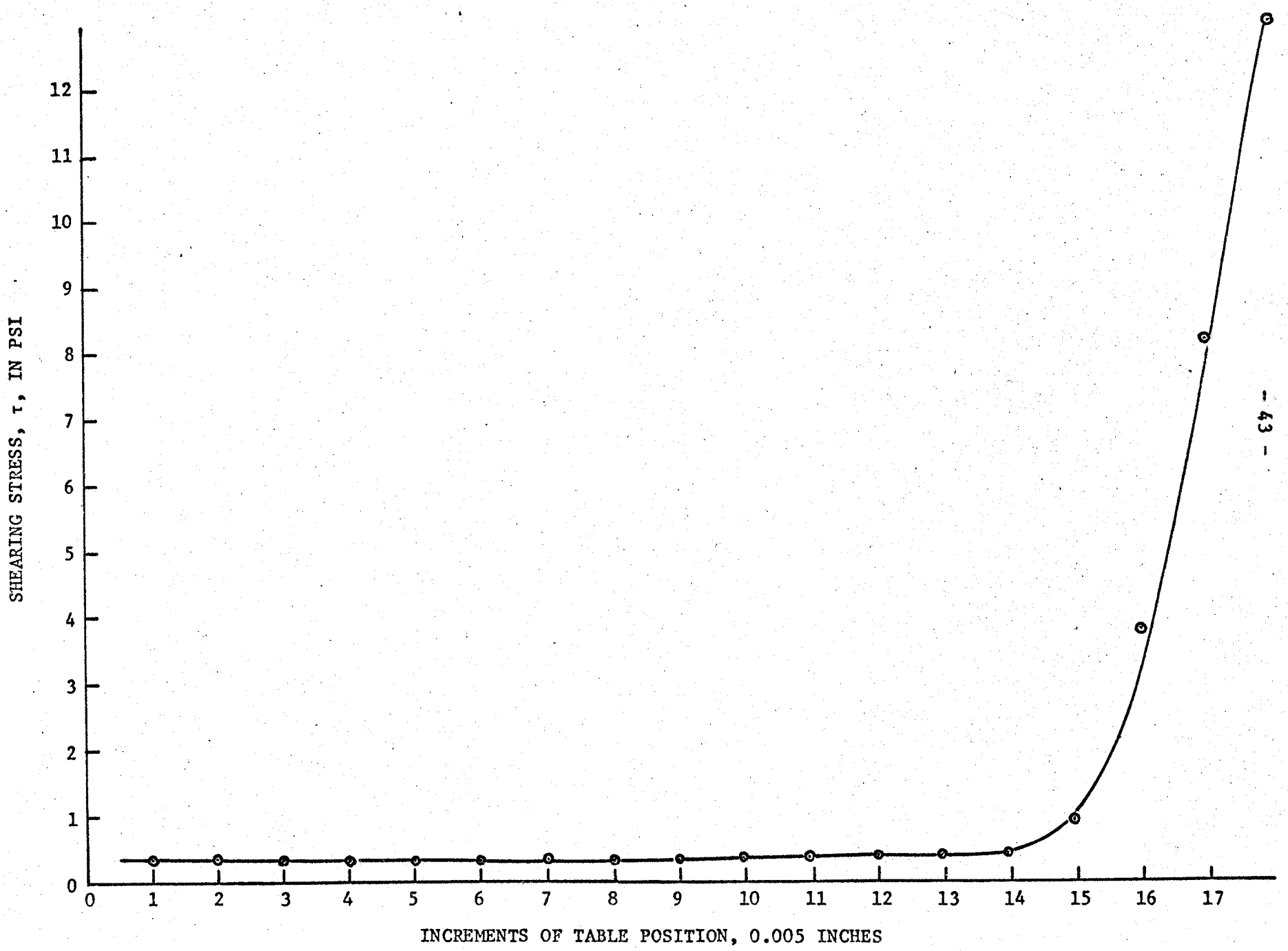
SHEARING STRESS, τ, IN PSI
0
1
2
3
4
5
6
7
8
9
10
11
12
0
1
2
3
4
5
6
7
8
9
10
11
12
13
14
15
16
17
INCREMENTS OF TABLE POSITION, 0.005 INCHES

TABLE I

DISPLACEMENT OF TABLE VS. SHEARING STRESS FOR FINER GRAINED SAND*

Table Position	(psi) Normal Stress	(psi) Shearing Stress
000		
005		
010		

005		
000	0	0.4
005	0.2	0.4
010	0.6	0.4
015	1.1	0.4
020	1.75	0.4
025	2.1	0.4
030	2.8	0.4
035	3.2	0.5
040	4.1	0.75
045	5.1	1.2
050	5.8	1.6
055	6.5	2.4
060	10.8	4.6
065	17.5	9.0
070	24.0	12.5

* $\tan \phi = \frac{\text{Shearing Stress}}{\text{Normal Stress}} \simeq 0.52$

TABLE II

DISPLACEMENT OF TABLE VS. SHEARING STRESS FOR COARSER GRAINED SAND*

Table Position	(psi) Shearing Stress
078.5	0.4
088.5	0.5
098.5	4.0
105.0	7.0

* $\tan \phi = \frac{\text{Shearing Stress}}{\text{Normal Stress}} \simeq 0.625$

TABLE III

DISPLACEMENT OF TABLE VS. SHEARING STRESS FOR GLASS BEADS*

Table Position	(psi) Normal Stress	(psi) Shearing Stress
095	0	0.25
100	0	0.38
105	0.15	0.36
110	0.4	0.36
115	0.4	0.35
120	0.4	0.35
125	0.4	0.35
005	0.2	0.35
010	0.1	0.37
015	0.2	0.35
020	0.4	0.35
025	0.2	0.37
030	0.2	0.4
035	0.35	0.4
040	0.4	0.4
045	0.2	0.4
050	2.2	0.9
055	12.5	3.8
060	27.0	8.2
065	40.0	13.0

* $\tan \phi = \frac{\text{Shearing Stress}}{\text{Load}} \simeq 0.305$

FIGURE XIV

SHEARING STRESS VS. PORE WATER PRESSURE

FOR FINER GRAINED SAND

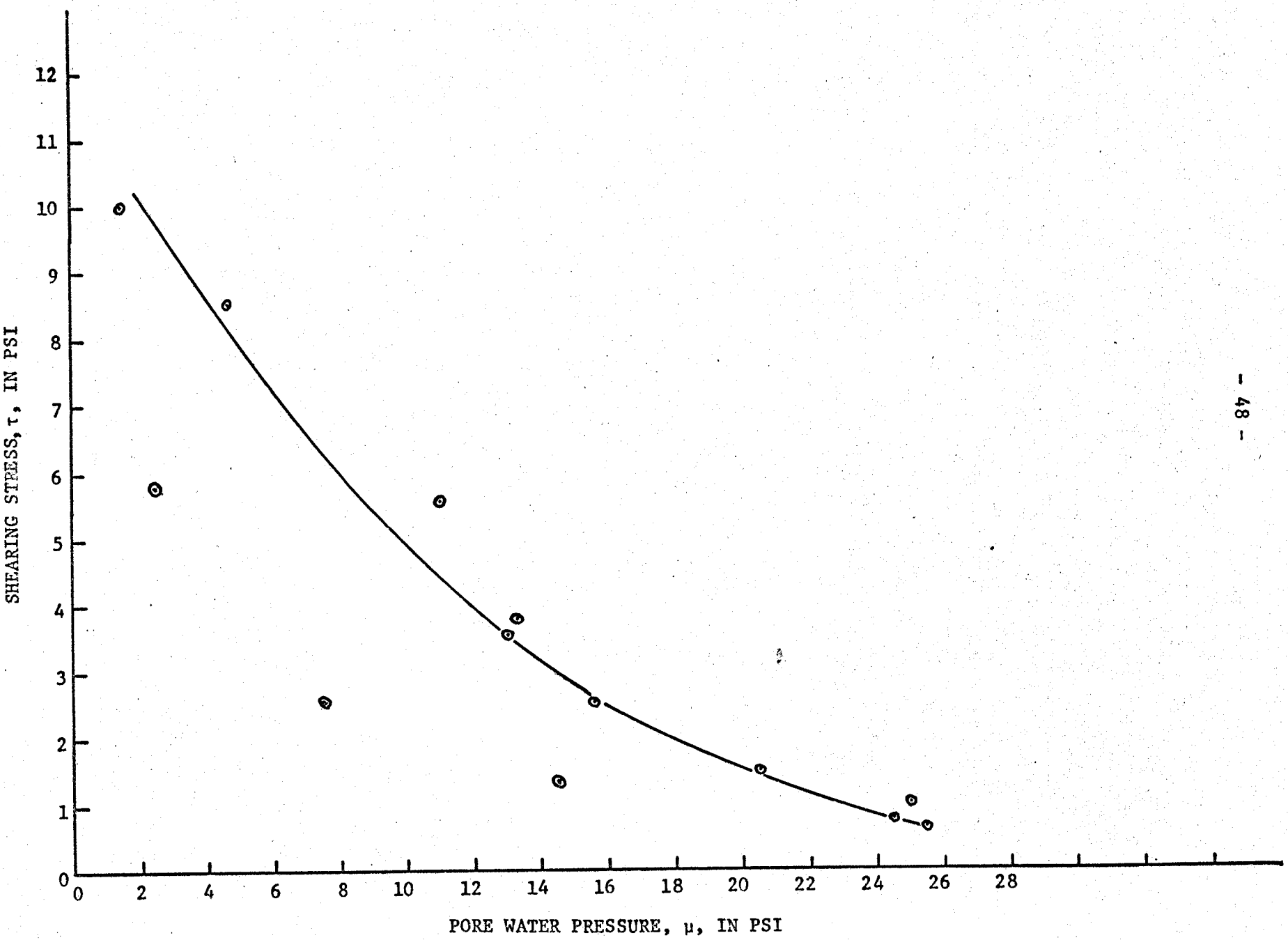
SHEARING STRESS, τ, IN PSI
0
1
2
3
4
5
6
7
8
9
10
11
12
0
2
4
6
8
10
12
14
16
18
20
22
24
26
28
PORE WATER PRESSURE, μ, IN PSI

FIGURE XV

SHEARING STRESS VS. PORE WATER PRESSURE

FOR COARSER GRAINED SAND

⊖	τ_{meas}	8 July
Δ	τ_{meas}	4 July

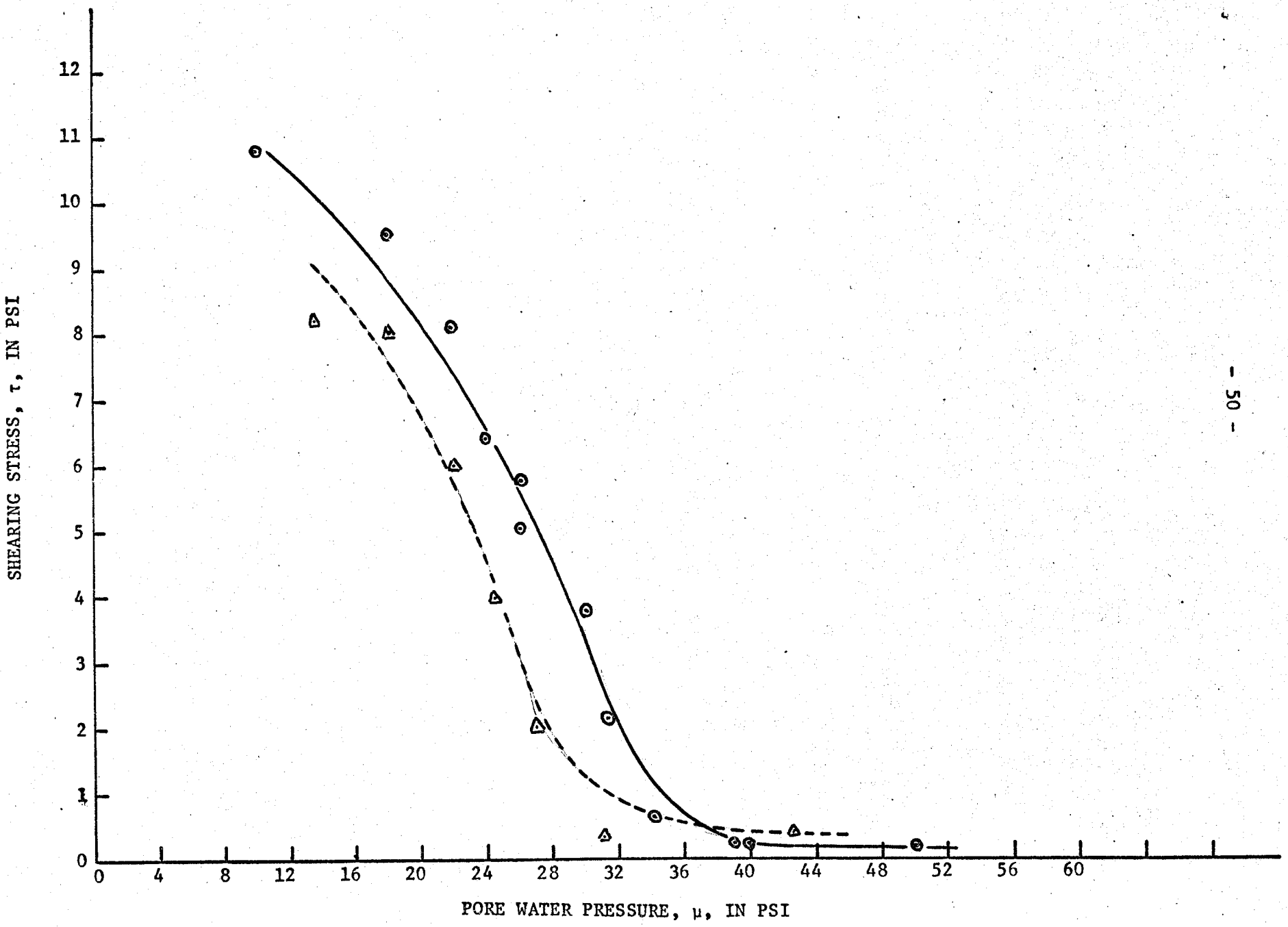
SHEARING STRESS, τ, IN PSI
0
1
2
3
4
5
6
7
8
9
10
11
12
0
4
8
12
16
20
24
28
32
36
40
44
48
52
56
60
PORE WATER PRESSURE, μ, IN PSI

FIGURE XVI

SHEARING STRESS VS. PORE WATER PRESSURE

FOR GLASS BEADS

⧈	τ_{pred}	Test 1
⊖	τ_{meas}	Test 1
▲	τ_{meas}	Test 2
◈	τ_{meas}	Test 3
X	τ_{meas}	Test 4

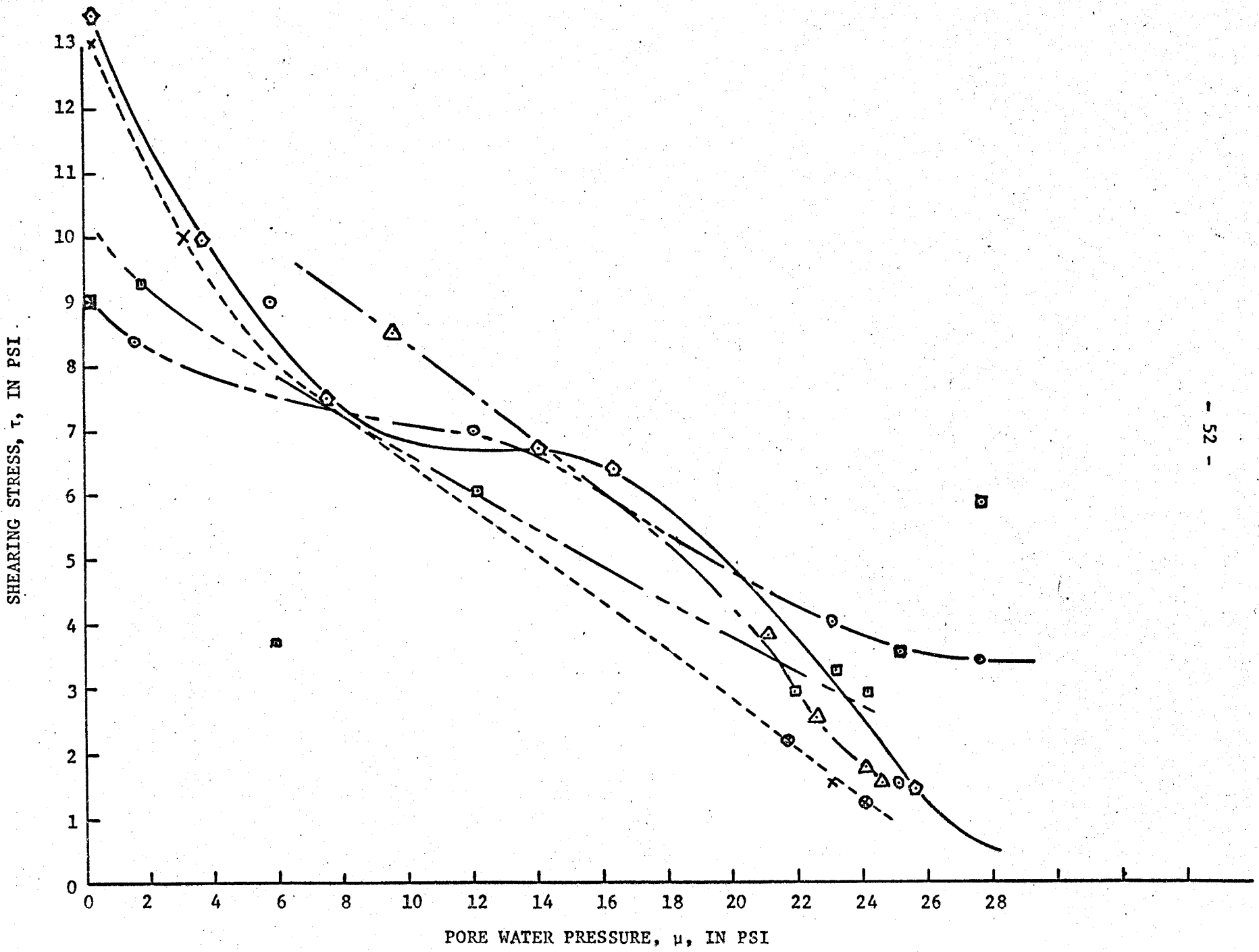
SHEARING STRESS, τ, IN PSI
PORE WATER PRESSURE, μ, IN PSI
0
1
2
3
4
5
6
7
8
9
10
11
12
13
0
2
4
6
8
10
12
14
16
18
20
22
24
26
28

TABLE IV

MEASURED AND PREDICTED SHEARING STRESS

VS. PORE WATER PRESSURE

FOR FINER GRAINED SAND

μ	t_{meas}	σ_t	$\sigma_e=\sigma_t-\mu$	τ_{pred}	$\tau_{pred}-\tau_{meas}$
25.5	0.6	34.2	8.7	4.52	+3.92
25.0	1.0	31.0	6.0	3.12	+2.12
24.5	0.8	33.0	8.5	4.42	+3.62
20.6	1.5	28.4	7.8	4.05	+2.55
15.6	2.5	26.0	10.4	5.4	+2.90
14.5	1.3	27.0	12.5	6.5	+5.2
13.3	3.75	25.0	11.7	6.09	+2.34
12.5	3.5	24.5	12.0	6.24	+2.74
11.0	5.5	24.0	13.0	6.76	+1.16
7.5	2.5	23.0	15.5	8.06	+5.56
4.75	8.5	21.0	16.25	8.43	-0.07
2.5	5.75	19.0	16.5	8.68	+2.93
1.5	10.0	20.0	18.5	9.63	-0.37

TABLE V

MEASURED SHEARING STRESS VS. PORE WATER PRESSURE

FOR COARSER GRAINED SAND

(Test 4 July)

μ	τ_{meas}
42.5	0.4
31.0	0.3
27.0	0.2
24.5	4.0
22.0	6.0
18.0	8.0
13.5	8.2

TABLE VI

MEASURED AND PREDICTED SHEARING STRESS

VS. PORE WATER PRESSURE FOR COARSER GRAINED SAND

(Test 8 July)

μ	τ_{meas}	σ_t	$\sigma_e=\sigma_t-\mu$	τ_{pred}	$\tau_{pred}-\tau_{meas}$
50.0	0.2	52.0	2.0	1.25	+1.05
40.0	0.19	44.0	4.0	2.5	+2.31
37.5	0.2	40.0	2.5	1.56	+1.36
34.0	0.6	35.0	1.0	0.625	+0.025
30.0	3.75	36.5	6.5	4.06	+0.31
29.0	2.1	32.75	3.75	2.34	+0.24
26.0	5.0	35.0	9.0	5.61	+0.61
26.0	5.75	34.25	8.25	5.16	-0.59
24.0	6.4	32.75	8.75	5.46	-0.94
22.0	8.2	32.0	10.0	6.25	-1.95
17.0	9.5	28.0	11.0	6.875	-2.63
10.0	10.75	24.0	14.0	8.75	-2.0
6.75	10.0	22.0	15.25	8.66	-1.34

TABLE VII

MEASURED AND PREDICTED SHEARING STRESS

VS. PORE WATER PRESSURE FOR GLASS BEADS

(Test #1, 10 July)

μ	τ_{meas}	σ_t	$\sigma_e=\sigma_t-\mu$	τ_{pred}	$\tau_{pred}-\tau_{meas}$
27.5	3.4	47.0	19.5	5.96	+2.56
25.0	3.5	36.0	11.0	3.63	+0.13
25.0	1.5	36.5	11.0	3.63	+2.13
24.0	1.25	33.0	9.0	3.0	+1.75
23.0	4.0	34.0	11.0	3.35	-0.65
21.75	2.2	33.0	9.0	3.0	+0.8
12.0	7.0	32.0	20.0	6.1	-0.9
5.75*	9.0	34.0	12.25	3.73	-5.27
11.5	8.4	32.0	30.5	9.3	+0.9
0.0	9.0	29.5	29.5	9.0	0

*Bad Data Point

TABLE VIII

MEASURED SHEARING STRESS

VS. PORE WATER PRESSURE

FOR GLASS BEADS

(Test Numbers 2, 3, and 4 - 10 July)

Test #2		Test #3		Test #4	
μ	τ_{meas}	μ	τ_{meas}	μ	τ_{meas}
24.5	1.5	25.5	1.4	24.0	1.25
24.0	1.75	16.25*	6.4	23.0	1.50
22.25	2.5	14.0*	6.75	21.75	2.20
21.0	3.8	7.5	7.5	3.0	10.0
9.5	8.5	3.75	10.0	0.25	13.0
		1.5	10.5		
		0.25	13.5		

*Bad Data Point

DISCUSSION OF RESULTS

The magnitude of reduction in shearing stress with an increase in pore water pressure varied from a fifty percent decrease for the coarser grained sand to about a ninety percent decrease for the glass beads and finer grained sand. The fifty percent value may be misleading however, as a further increase of only 10 psi resulted in a great reduction of shearing stress to the point that it was only 10 percent of the initial value.

No doubt, part of the explanation for all of this great decrease lies with Coulomb's Effective Stress Law. However, in view of the fact that the coefficient of friction did not remain constant, but seemed to decrease with increasing pore water pressure leads one to believe that perhaps there may have been formed a layer of water of small thickness between the sample and bottom surface of the top plate assembly. There was physical evidence to sbustantiate this hypothesis. Upon the completion of a particular test and the lowering of the table, it was noticed that there was a depression (i.e., decrease in sample thickness) around the source and sink of about one fourth inch.

Also, considering the fact that the area of the top plate assembly was roughly 55 square inches, with a pore water pressure of 25 psi acting on the plate, one gets a total load of about 1400 pounds. As has been previously stated, the system was not completely rigid (see Figs. VII and IX), and from a test conducted on 11 july, this non-rigidity was somewhat quantitized (See Table IX, Appendix). The top plate assembly was supported at only one point in the middle when attached to the milling machine and may have "bowed" upward when subjected to high pressure.

Although it was intended to make the dynamometer as rigid as possible, a small amount of deflection was inevitable. In this case there was probably a separation, however slight, of the top and bottom plate assembly with the insertion of a small disc of water in the increased volume. The sand was likely compacted from the start of testing, by virtue of the fact that in raising the table into position there was no pore water pressure. Also, if nothing else, rotation of the sample would have evened and compacted it. Further, the grains of sand near the upper and lower surfaces were most likely ground up, decreasing the effective coeffecient of friction. In all of the tests it was noted that the shearing stress decreased after a period of time apparently for this very reason.

In the Recommendations, one will note that either a very stiff spring or a hydraulic load should be applied for support rather than a "rigid" body as used in the experimentation of this report. No doubt the shearing stress would have decreased with an increased pore water pressure, but probably not to the same extent as noted in the results.

CONCLUSIONS AND RECOMMENDATIONS

The possibility of aiding the removal of a grounded ship may exist in using high water pressure pumped from the ship to the supporting soil. Although not conclusive, it was found that the flow rate did not greatly influence the reduction in shearing stress. Of course, the theory (the Effective Stress Law) would tell one the same thing, but it was felt at the beginning of experimentation that perhaps flow would play a greater role.

Further, results of the testing on the three different samples showed that the shearing stress effectively went to zero regardless of the coefficient of friction. Granted, this may have been due to a lifting of the dynamometer off of the sample, but who is to say that this would not be the case in a real situation?

The results of the deflection test (see Appendix, Table IX), may have led one to the conclusion that perhaps the dynamometer was lifted from the sample. This possibility points up to the fact that a very stiff spring or hydraulic coupling be used to support the top plate assembly so as to maintain a constant load on the sand sample.

Recall however, that the system was quite stiff (on the order of 10^5 lb/in), thus simulating somewhat the same resistance to motion that a heavy ship would have. Another recommendation evolves from this point, since in any future investigation this very test should be made. That is, a model of a ship should be placed in a bed of water waturated sand, and a test be made of deflection vs. water pressure. However, the sample should be smoothed out and stirred up so as to keep the grain size even from test to test without the grinding down to a smaller grain size.

The coefficient of permeability was not a factor in this report as the pore water pressure was monitored as to its pressure without regard to head loss due to highly impervious soil. Thus, if a fixed input of 25 psi were used, and the head loss not corrected for, then the impermeability would have been considered and the test made more meaningful. However, as the output (in psi) of the Cambridge City water varied, this could not be done with the apparatus set up as it was.

More tests should be made on several types of sand and some cohesive soils. Certainly working with cohesive soils is not as clean nor as simple as with sand, but then one generally does not have much choice concerning the type of soil on which his ship runs aground. Finally, it was noted that some of the aluminum from the top plate assemply in the form of flakes was found in the soil sample and the effect of this contamination on shearing stress should be considered.

As a final conclusion, the rate of shear did not influence the magnitude of shearing stress. However, for a tug with a fixed bollard power, there is a limit on the rate of shear.

Perhaps the next step for anyone who wishes to pursue this matter further is to set up a tow tank apparatus and actually measure the drag for various water pressures. Feasibility has not been mentioned before, as in this test it was not really considered. It would be necessary for a marine engineer to investigate the feasibility of mounting pumps, fittings, etc., on the hull of a ship simply for the purpose of running aground. No doubt the only type ship for which this idea would be worthwhile would be an LST (Landing Ship Tank or similar landing craft).

Further, higher pressures and greater weights should be used to more closely simulate an actual salvage operation. Modeling an infinitely

long ship with an annular ring of sources was a poor attempt to approximate the practical situation. This finally leads to the recommendation that one should more closely adhere to all of the boundary conditions which in one way or another were compromised. In short, the recommendation is made that any further investigation should be modeled as close as possible to the real case, but on a smaller scale.

Finally, the case of a periodic flow rate (e.g., sinusoidal) be considered where both the amplitude and frequency are varied. Gordon found that by vibrating the sample the shearing resistance decreased [4], and perhaps the same would be observed for an oscillating flow rate.

BIBLIOGRAPHY

1. Capper, P. L. and Cassie, W. F., The Mechanics of Engineering Soils, pp. 97, 98, 195.
2. Cook, Nathan H. and Rabinowicz, Ernest, Physical Measurement and Analysis, pp. 153-167, 143-149.
3. De Ridder, N. A., "Comparative Study on Hydraulic Conductivity of Unconsolidated Sediments," Journal of Hydrology, Vol. 3, No. 3-4, 1965, pp. 180-206.
4. Gordon, Samuel J., private communication, M.I.T., 1968.
5. Gordon, Samuel J., "Soil-Solid Friction Dynamometer, Description and Calibration Results," Ph.D. Thesis Report, Department of Mechanical Engineering, Massachusetts Institute of Technology.
6. Jacob, C. E., "Flow of Ground Water," Engineering Hydraulics, Proceedings of the Fourth Hydraulics Conference, Iowa Institute of Hydraulic Research, June 12-15, 1949, Hunter Rouse, ed., pp. 321-385.
7. Leonards, G. A., "Experimental Study of Static Friction and Dynamic Friction between Soil and Typical Construction Materials," AFWL-TR-65-161, December, 1965, Purdue University.
8. Plummer, F. L., Notes on Soil Mechanics and Soil Foundations, p. 56.
9. Sanborn Company, Waltham, Mass., Sanborn Dual Channel Carrier-Amplifier Recorder Model 321 Instruction Manual, pp. 1-16.
10. Sanborn Company, Waltham, Mass., Sanborn Dual Channel Carrier Amplifier Recorder Model 60 Instruction Manual, pp. 1-18.
11. Schaevitz-Bytrex, Inc., Waltham, Mass., HFD Series Pressure Transducers, Instruction Manual, pp. 1-8.
12. Terzaghi, Karl and Peck, Ralph B., Soil Mechanics in Engineering Practice, pp. 40-51.

OTHER REFERENCES

1. Bazant, Zdenek, "Stability of Saturated Sand During Earthquakes," Proceedings of the Third World Conference on Earthquake Engineering, 1965 Vol. I, pp. 16-19.

2. Biot, M.A., "Theory of Propagation of Elastic Waves in a Fluid Saturated Porous Sand," The Journal of the Acoustical Society of America, Vol. 28, No. 2, March 1956, pp. 168-191.

3. Converse, Fredrick J., "Compaction of Sand at Resonant Frequency," Symposium on Dynamic Testing of Soils, American Society for Testing Materials, Special Technical Publication No. 156, July 2, 1953, pp. 124-138.

4. D'Appolonia, Elio, "Loose Sands - Their Compaction by Vibroflotation," Symposium on Dynamic Testing of Soils, American Society for Testing Materials, Special Technical Publication No. 156, July 2, 1953, pp. 138-155.

5. Florin, V. A. and Ivanov, P. L., "Liquefaction of Saturated Sandy Soils," Proceedings of the Fifth International Conference of Soil Mechanics and Foundation Engineering, 1961, Vol. I, pp. 107-111.

6. Hamilton, E. L., Shumway, G., Menard, H. W., Shipek, C. J., "Acoustic and Other Physical Properties of Shallow-Water Sediments off San Diego," The Journal of the Acoustical Society of America, Vol. 28, Nos. 1-6, 1956, pp. 1-15.

7. Lee, Kenneth E and Seed, H. Bolton, "Liquefaction of Saturated Sands during Cyclic Loading," Journal of the Soil Mechanics and Foundations Division, American Society of Civil Engineers, Vol. 92, No. SM6, November 1966, Proceedings Paper 4972, pp. 105-134.

OTHER REFERENCES (Continued)

8. Lee, Kenneth E. and Seed, H. Bolton, "Cyclic Stress Conditions Causing Liquefaction of Sand," Journal of American Society of Civil Engineers, Vol. 92, No. SM 1, January 1967, Proceedings Paper 5058, pp. 47-70.

9. Maslov, N. N., "Questions on Seismic Stability of Submerged Sandy Foundations and Structures," Proceedings of the Fourth International Conference on Soil Mechanics and Foundation Engineering, Vol. 1, 1957, pp. 368-375.

10. Mogami, T., "The Behavior of Soil during Vibration," Proceedings of the Fourth International Conference on Soil Mechanics and Foundation Engineering, Vol. 1, 1957, p. 152.

APPENDIX

By referring to Fig. XVII one will note that the Appendix is arranged in a somewhat similar manner to the block diagram. That is, the specifications, sample calculations, etc., will be concerned with those items that are located in the "Sensing" area of the diagram. This makes up the bulk of the Appendix. Following that discussion, the "Display" area was considered and will be found to be rather short in length.

SENSING

Specifications for Pore Water Pressure Transducer [11]

Manufacturer:	Schaevitz-Bytrex, Inc.; Waltham, Mass.
Transducer Serial No.:	13450
Model No:	HFD 25
Capacity:	25 PSI
Sensitivity Factor:	6.63 mV/V
Excitation Voltage:	25 Volts
Lowest Natural Frequency:	60 KC
Diaphragm Deflection:	60×10^{-6}" (maximum)

Specifications for SR4 Strain Gages (See Fig. XVIII and XIX)

Manufacturer:	BLH Electronics, Waltham, Mass.
Type:	A-8, Bonded Resistance
Resistance:	120.5 ± 0.3 Ohms
Gage Factor:	$1.83 \pm 2\%$
Lot No.:	B-31

Load Cell - Description and Stiffness Calculation

Four octagonally shaped, two dimensional load cells were mounted upon the middle circular annulus with the top and bottom secured.

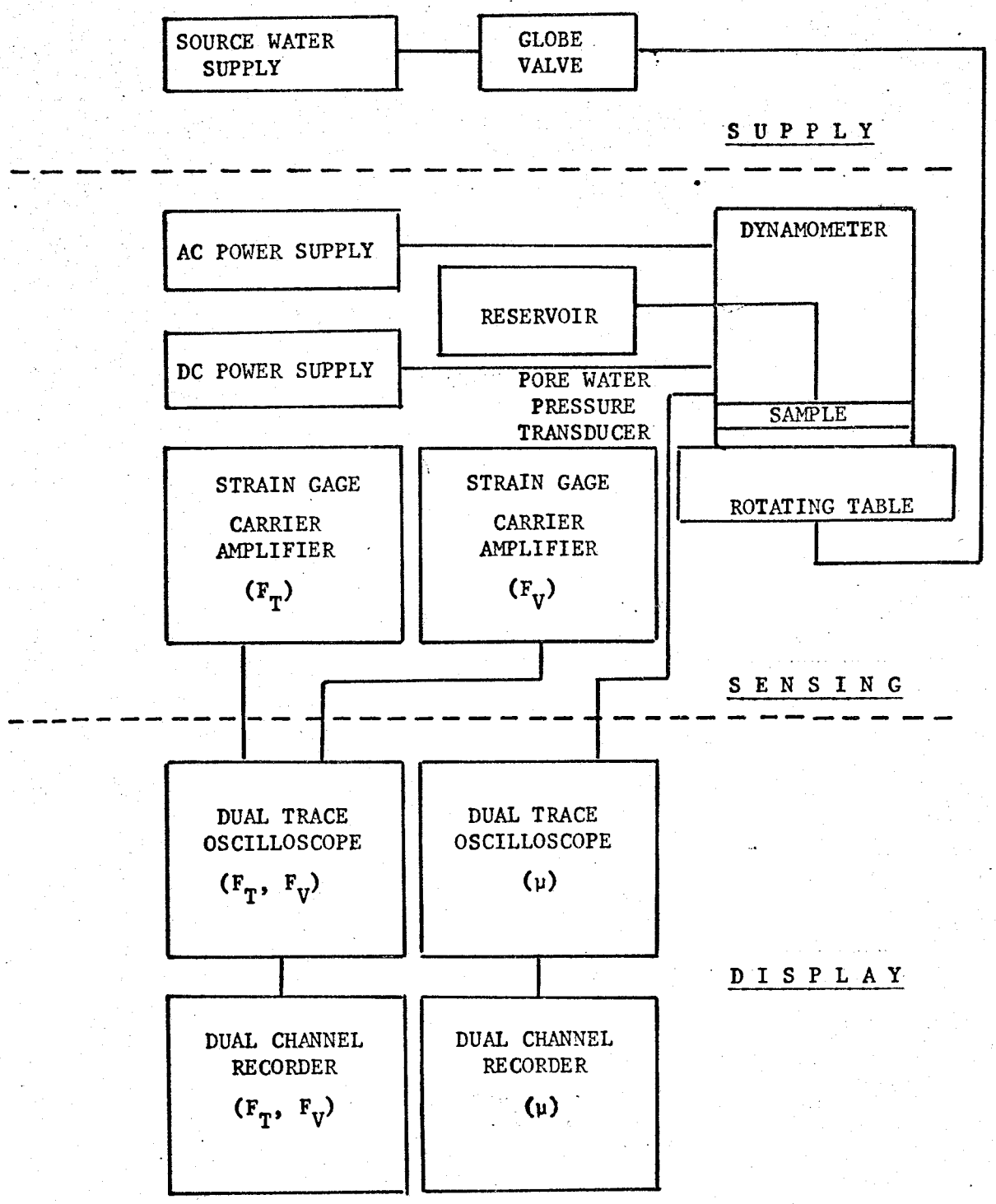

FIGURE XVII

BLOCK DIAGRAM OF FRICTION DYNAMOMETER

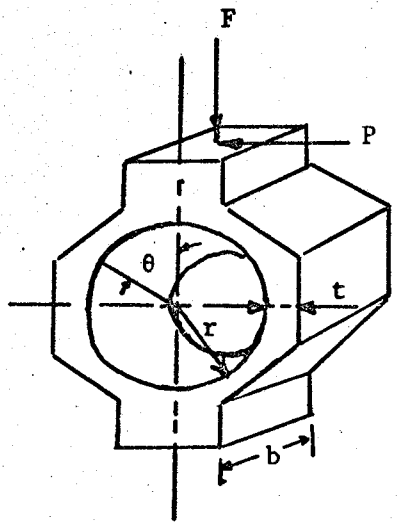

Dimensions:

$t = 0.106$ in.

$b = 0.750$ in.

$r_{mean} = 0.500 + \frac{0.106}{2}$

$= 0.553$ in.

FIGURE XVIII

TWO DIMENSIONAL LOAD CELL (RING TYPE) [5]

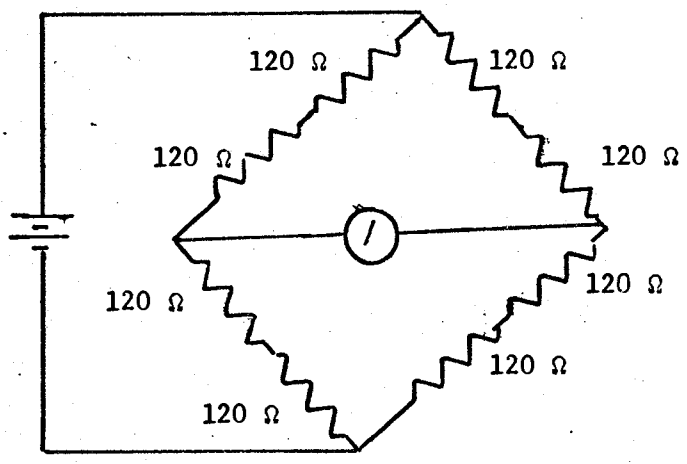

Strain Gage Specification:

Resistance = 120 ohms

Gage Factor = 1.83

BLH SR4 Type A8

FIGURE XIX

SCHEMATIC OF WHEATSTONE BRIDGE OF LOAD CELL [5]

See Fig. XVIII and XIX. LCDR. S. J. Gordon designed and built the unit which is similar to the type of dynamometer marketed by Cook, Smith, and Associates of M.I.T.

The octagonal shape was selected because of the reduced tendency to roll when a horizontal load was applied. By mounting sixteen strain gages on the four load cells (four strain gages to a load cell), the unit was then capable of measuring independently the vertical and horizontal deflections which could be recalculated as normal and shearing stress. The strain gages that were attached to the individual load cells were connected in a four active arm wheatstone bridge. By applying either a normal or shearing load on the face of the middle annulus, an imbalance resulted which produced a signal directly proportional to the applied load. The strain gages which measured shear were placed at strain nodes for axial deflection, while those which measured normal load were placed at strain nodes for shear deflection [5]. Although not solvable by analytical means, strain nodes have been empirically determined by photoelastic means to occur at $\theta = 50°$ and $\theta = 90°$. [2, p.162].
The strain and deflection equations governing are approximated by: [2, p.163]

$$\varepsilon_{50°} \simeq 1.4\frac{Pr}{Ebt^2} \qquad (19)$$

$$\varepsilon_{90°} \simeq 0.7\frac{Fr}{Ebt^2} \qquad (20)$$

$$\delta_p \simeq 3.7\frac{Pr^3}{Ebt^3} \qquad (21)$$

$$\delta_f \simeq 1.0\frac{Fr^3}{Ebt^3} \qquad (22)$$

The load cells used in this report had the following dimensions:

$t = 0.106$ in. = thickness

$r = 0.553$ in. = mean radius

$b = 0.750$ in. = width

$E = 30 \times 10^6$ lb/in^2 = modulus of elasticity for steel

The following results listed were part of an attempt to check for the actual stiffness of the ring compared to the theoretical stiffness. The deflection of the apparatus was measured when loaded to 25 lb/in^2 from which a "measured" stiffness was calculated. This "measured" stiffness was then compared to a "theoretical" stiffness based on Eqn. (22).

TABLE IX

DEFLECTION TEST USING 25 PSI PORE WATER PRESSURE

Dial Indicator from Top of Milling Machine
On the Outer Annulus

		Deflection
1.	Behind Pore Pressure Transducer Midway Between Two Supports	0.0015 in.
2.	Next to Support	0.002 in.

Dial Indicator from Base of Milling Machine
On the Middle (Load Cell) Annulus

1.	Behind Pore Pressure Transducer Midway Between Two Supports	0.006 in.
2.	Next to Support	0.006 in.
3.	Top of Milling Machine	0.007 in.
4.	On Pore Pressure Transducer	0.007 in.
5.	Middle of Annulus Next to Load Cell	0.007 in.

For any force measuring device, the following well known equation is applicable:

$$F = k\delta \tag{23}$$

where F = load in lbs.

k = stiffness in lbs/in.

δ = deflection in in.

Thus the "measured" value of k is as follows:

Area of annulus $\simeq$ 15 in^2

Pressure, μ $\simeq$ 25 lb/in^2 over annulus only

Deflection, δ $\simeq$ 0.0015 in. (Note that the dynamometer was not completely rigid, and thus the deflection of one plate with respect to the other is the only δ considered.)

$$F = 25\ lb/in^2 \times 15\ in^2 = k\delta$$

therefore

$$k = \frac{25\ lb \times 15}{0.0015\ in.} = 250 \times 10^3\ lb/in.$$

$$k = 2.5 \times 10^5\ lb/in \text{ "measured" stiffness}$$

The "calculated" value of k is as follows:

$$k \text{ for one load cell} = \frac{F}{\delta_f} = \frac{Ebt^3 \times F}{Fr^3}$$

$$= \frac{30 \times 10^6\ lb/in^2 \times 0.750\ in \times (0.106\ in)^3}{1.0 \times (0.553\ in)^3}$$

$k = 15.8 \times 10^4$ lb/in for one load cell

$k = 6.32 \times 10^5$ lb/in for four load cells "calculated" stiffness.

Thus the "calculated" stiffness is found to be about 2.5times that of the "measured" stiffness. The subject of deflections is dealt with in greater detail in the Discussion of Results and the Conclusion.

In discussing the calibration of the dynamometer, the first two equations of this Appendix must be considered: (Eqn. 19 and 20)

$$\varepsilon_{50°} = \frac{1.4P(0.553 \text{ in})}{30 \times 10^6 \text{lb/in}^2 (0.750 \text{ in})(0.106 \text{ in})^2}$$

$$= \frac{3.061 \times 10^{-6} P}{\text{lbf}}$$

or

$$\frac{\varepsilon_{50°}}{P} = \frac{3.061 \ \mu\varepsilon}{\text{lbf}} \quad \text{(Predicted)}$$

similarly,

$$\frac{\varepsilon_{90°}}{F} = \frac{1.5305 \ \mu\varepsilon}{\text{lbf}} \quad \text{(Predicted)}$$

Thus for a total axial load of 1 pound (about 0.0665 lbf/in^2) the predicted strain would be:

$$\varepsilon_{50°} = 3.06 \ \mu\varepsilon = 3.06 \text{ microstrain units}$$

Likewise, for a total applied shearing load of 1 pound,

$$\varepsilon_{90°} = 1.53 \ \mu\varepsilon = 1.53 \text{ microstrain units}$$

To check these values when he constructed the dynamometer, Commander Gordon performed a calibration test using dead weights to load the sensing elements for which the results will be repeated here. By applying tangential and normal forces with a system of levers and pulleys to the dead weights, the measured strain indications were:

$$\epsilon_{50°} = 12.0\ \mu\epsilon$$

$$\epsilon_{90°} = 24.2\ \mu\epsilon$$

Thus the measured strain values were ascertained to be about 0.8 of the predicted values. Note, that in both cases, the ratio of tangential shear to axial shear was almost the same. Gordon found the response to be linear throughout the test, as indicated in the calibration curves which follow. Gordon likewise found that cross interference, that is an axially applied load causing shear strain and vice versa, was negligible. (See Fig. XX and XXI.)

The calibration of normal and shearing stress was also solved analytically. From p.11 of the Sanborn Model 321 Instruction Manual [9]:

$$\text{Strain} = (\text{division deflection}) \times (0.1) \times (\text{basic sensitivity}) \times (\text{attenuator}) \quad (24)$$

The interest centered on how many divisions deflection of the stylus in the Sanborn recorder one would get for a normal applied loading of say 1 $lb/in.^2$ The following information was also given in the Manual:

Strain represented by ten divisions deflection
at attenuator setting 1 = 10 microinches/inch

Basic sensitivity = 40

FIGURE XX

CALIBRATION CURVE

FOR AXIAL LOAD

	Attenuator	lb/cm
X	10	8.3
⊖	20	16.7
Δ	50	43.2

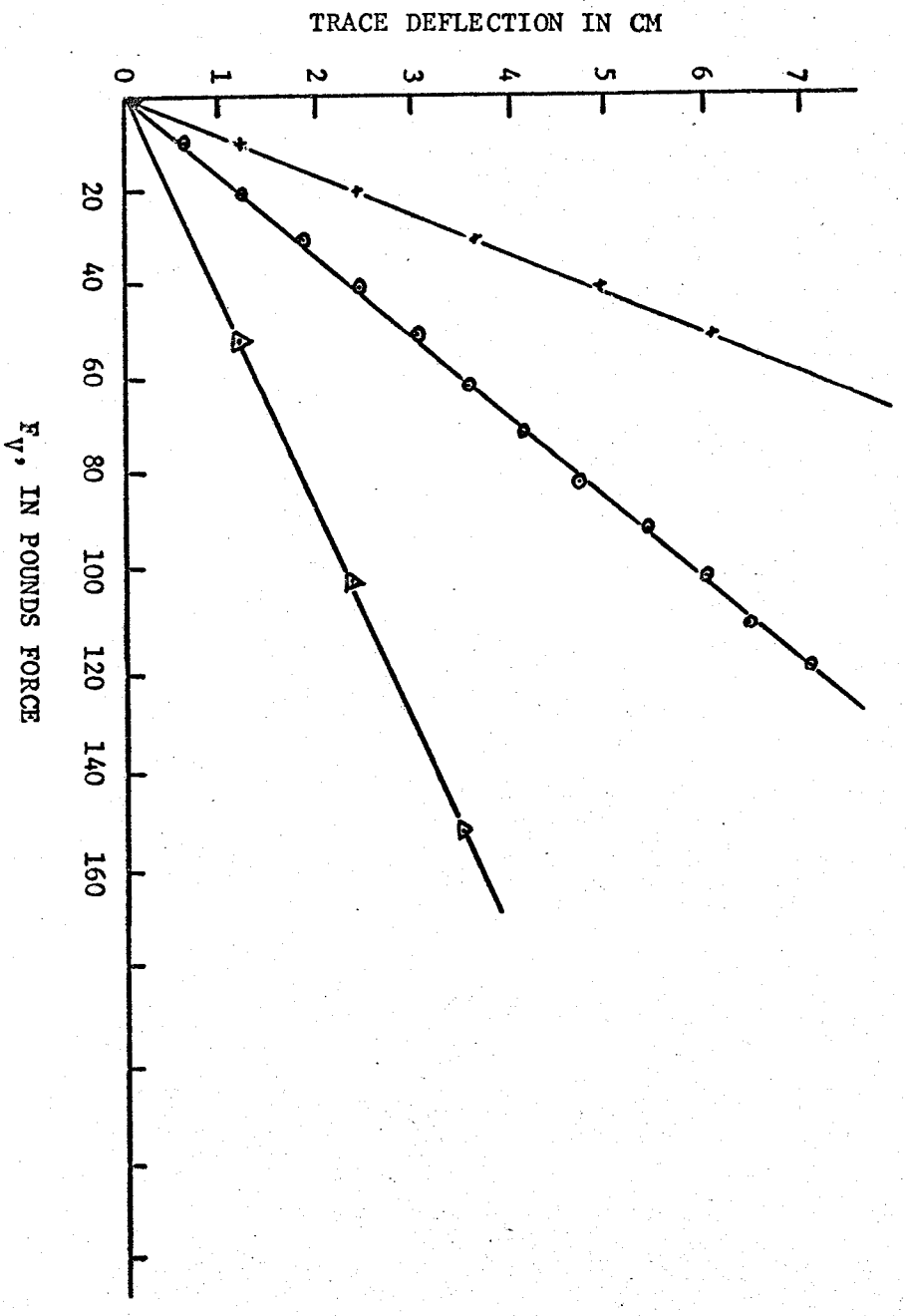
TRACE DEFLECTION IN CM
0
1
2
3
4
5
6
7
20
40
60
80
100
120
140
160
F_V, IN POUNDS FORCE

FIGURE XXI

CALIBRATION CURVE

FOR TANGENTIAL LOAD

	Attenuator	lb/cm
⊖	50	21.5
Δ	100	42

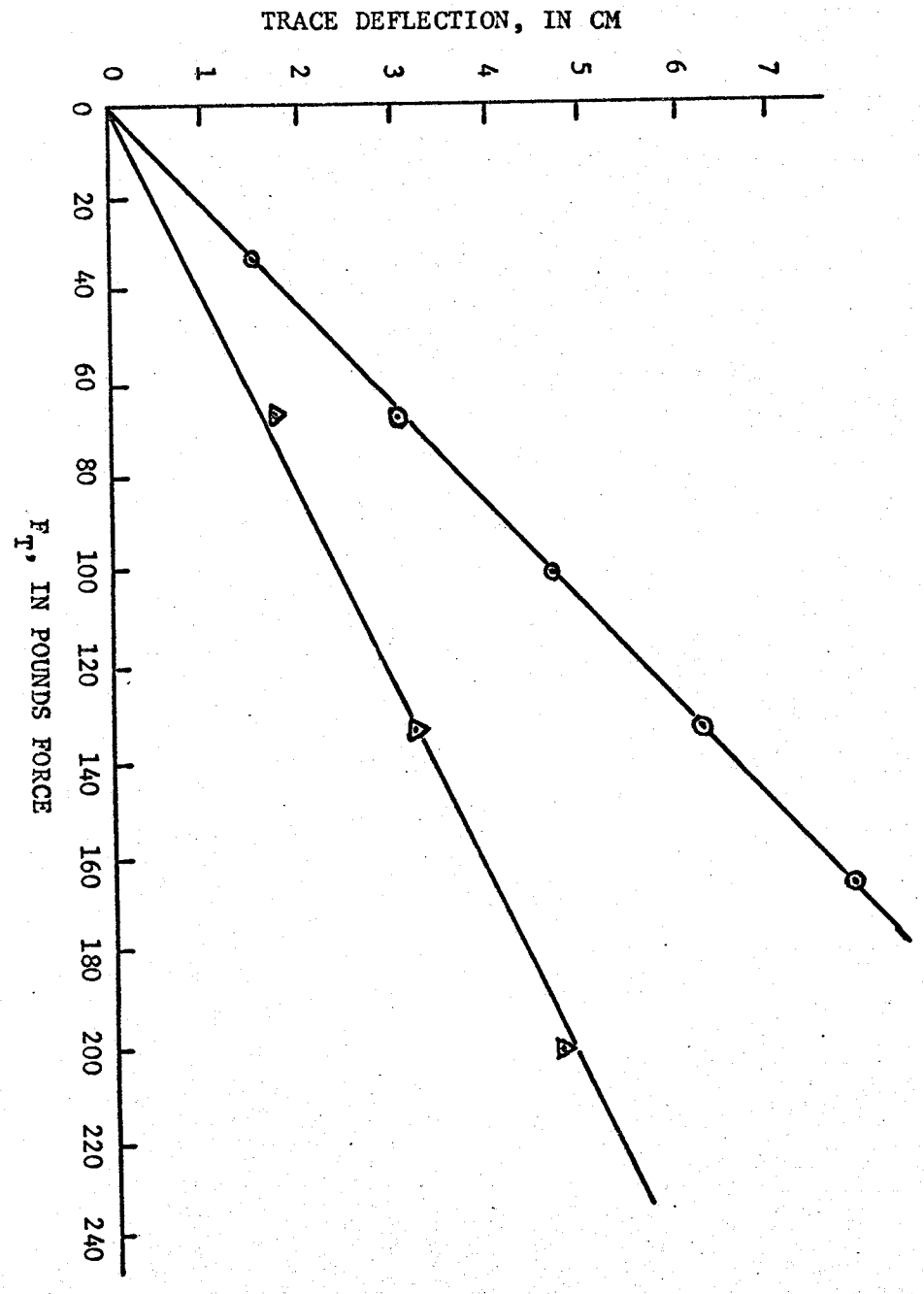
TRACE DEFLECTION, IN CM
0
1
2
3
4
5
6
7
F_T, IN POUNDS FORCE
0
20
40
60
80
100
120
140
160
180
200
220
240

Solving for the number of divisions deflection for a normal loading of 1 psi at attenuator 1:

$$\text{Division deflection} = \frac{\text{Strain}}{(0.1)} \times \frac{1}{\text{attenuator setting}} \times \frac{1}{\text{basic sensitivity}}$$

$$\text{Area of annular ring} = 15 \text{ in}^2$$

Therefore

$$\text{Strain} = \varepsilon_{90°} = \frac{1.53 \ \mu\varepsilon}{\text{lbf}} \times 15 \text{ in}^2 \times 1 \text{ lbf/in}^2$$

and

$$\text{Division deflection} = \frac{1.53 \ \mu\varepsilon \times 15}{(0.1)(40)(1)} \times \frac{1}{10 \ \mu \text{ inches/inch}}$$

$$= 5.75 \text{ divisions deflection (in mm)}$$

However, in the actual testing, in an effort to simplify the measurements, a normal stress of 1 psi would be assumed at 5 divisions deflection (0.2 psi/mm).

Similarly for shearing stress at attenuator 1 for a stress of 1 psi:

$$\text{Strain} = \varepsilon_{50°} = \frac{3.06 \ \mu\varepsilon}{\text{lbf}} \times 15 \text{ in}^2 \times 1 \text{ lbf/in}^2$$

and

$$\text{Division deflection} = \frac{3.06 \ \mu\varepsilon \times 15}{(0.1)(40)(1)} \times \frac{1}{10 \ \mu \text{ inches/inch}}$$

$$= 11.50 \text{ divisions deflection (in mm)}$$

Likewise, in the actual testing, to simplify matters, a shearing stress of 1 psi would have been assumed after 10 divisions deflection of the stylus of the recorder (0.1 psi/mm).

Commander Gordon also calibrated the pore water pressure transducer for both the static and dynamic case. By applying a hydrostatic pressure to a volume of water enclosed by the sand sample chamber and noting the deflection of an oscilloscope trace of the transducer output, Gordon calibrated the transducer for the static condition. Compared simultaneously to the transducer output was both the height of a mercury manometer and the normal load sensing circuit of the dynamometer. From the results of this test, the transducer output was found to be slightly less (3.3%) than that measured by the manometer and dynamometer.

Although it was of no concern in the experimentation of this report, Gordon tested the dynamic response of the pressure transducer by comparing the output of the transducer to that of the dynamometer over a frequency of 5 to 600 cps. The transducer was found to be reliable up to 150 cps.

Finally, the pore water pressure had to be corrected for an excitation voltage different than 22.5 volts. From page 5 of the instruction manual

$$P_u = \frac{P_c \times E_o \times 10^3}{E_a \times S} \qquad (25)$$

where P_u = unknown pressure

P_c = capacity pressure = 25 psi

E_a = excitation voltage = 22.5 volts (ideally)

E_o = output voltage

S = sensitivity = 6.63 mV/V (applied at P_c = 25 psi)

Thus the excitation voltage had to be checked before and after each test and corrected according to the following equation:

$$P_u = \frac{(P_u \text{ measured})(22.5)}{(E_a \text{ measured})} \qquad (26)$$

TABLE X

SPECIFICATIONS FOR U.S. STANDARD SIEVE SERIES SAND STRAINERS

Manufacturer:	Macalaster Scientific Corporation, Cambridge, Mass.
Sieve No:	20
Opening:	0.0331 in. 0.84 mm
Manufacturer:	Newark Wire Cloth Company, Newark, New Jersey
Sieve No:	40
Opening:	0.0165 in. 0.42 mm
Manufacturer:	Newark Wire Cloth Company, Newark, New Jersey
Sieve No:	60
Opening:	0.0098 in. 0.25 mm

DISPLAY

Specifications for Sanborn Recorders

1. Model 321:

Manufacturer:	Sanborn Company, Waltham, Mass.
Sensitivity:	Nominal sensitivity of a 100 ohm four arm bridge is 10 microvolts of signal for one division of writing arm deflection.
Calibration:	Internal; 40 microvolts/volt excitation, $\pm$ 1%.
Excitation:	Supplied to the transducer by the recorder; 4.5 to 5 volts (not adjustable), 2400 cycles $\pm$ 2%.
Transducer Impedance:	Including other bridge components; a minimum of 100 ohms and a maximum of 5000 ohms (in this case 240 ohms).

2. Model 60:

Manufacturer:	Sanborn Company, Waltham, Mass.
Sensitivity:	10 mA output (or 1 cm on recorder) for a resistance change of 100 parts per million in one arm of bridge, normal sensitivity.
Excitation:	Excitation voltage delivered by the oscillator to the bridge is approximately 3.5 volts rms.
Transducer Impedance:	When using a complete four element transducer, the transducer resistance may have a value between 50 and 500 ohms.

TABLE XI

SENSITIVITIES OF THE RECORDER AND OSCILLOSCOPE

	Gain	Recorder	Oscilloscope
Normal Stress (σ_t)	25 mm	0.2 psi/mm at ATTN 1	2.28 psi/cm at 0.5 V/cm
Shearing Stress (τ)	23.2 mm	0.1 psi/mm at ATTN 1	1.14 psi/cm at 0.5 V/cm
Pore Water Pressure (μ)	V_T=22.5 V	0.5 psi/mm at ATTN 1	2.8 psi/cm at 10 V/cm